

Supporting Information of

The phase stability of the pentazole derivate compounds under high pressure

Xin Huang,^a Panpan Wu,^a Longjiu Cheng,^a Jianguo Zhang,^{*c} and Kun Wang^{*a,b}

^aDepartment of Chemistry, Anhui University, Hefei, Anhui 230601, P. R. China

^bKey Laboratory of Structure and Functional Regulation of Hybrid Materials (Anhui University), Ministry of Education; Hefei, Anhui 230601, P. R. China

^cState Key Laboratory of Explosion Science and Technology, Beijing Institute of Technology, Beijing 100081 P. R. China

Contents

1. Relationship of molecular structure-property.....	1
1-1. Dated optimized gas-phase structures under M062x/6-311+G(d,p).....	1
1-2. The vibrational frequencies of the four optimized gas-phase structures	2
1-3. Optimized molecular structures with the typical bond length (Å), Wiberg bond index (WBI), Natural bond orbital charge (NBO), and bond angle (°).	3
1-4. Molecular softness	4
2. Prediction of crystal structures based on Monte-Carlo method	5
2-1. Details of crystal structures predictions	5
2-2. The benchmark calculation of the different Forcefield.	11
3. Crystal structures.....	12
3-1. Test for the convergence criteria in crystal optimization.....	12
3-2. k-point test and cut-off test	13
3-3. Optimized crystal structures of pentazole derivate compounds	15
3-4. Lattice energy	18
3-5. Phonon calculation	19
4. Formation enthalpy	20
4-1. Formation of enthalpy of gas phase	20
4-2. The sublimation enthalpies of condensed-phase.....	20
4-3. The solid formation enthalpy ($\Delta_f H_{\text{solid}}$)	22
5. Structure-pressure relationship.....	23
5-1. Crystal elastic constants and mechanical stability	23
5-2. The calculated Lattice Parameters, Density, Volume, Total Energy of four crystals in the range of 0~200 Gpa	25
5-3. Typical atom charges in four crystals under different pressures (0~200 Gpa).....	28
5-4. Band gaps of four crystals under different pressures (0~200 Gpa).....	29
5-5. Structure change of four crystals under different pressures (0~200 Gpa).....	30
5-6 Formation Gibbs free energy (defined) at ambient and high pressure.	32
6. Molecular dynamics simulations with NPT ensemble	33
6-1. Atomic charges of the four structures preparing for MD simulation at ambient pressure.....	33
6-2. Energy-time curves of the four predicted crystals at ambient pressure (300 K and 500 K).....	34
6-3. The converged dynamic temperature of the four crystals at the pressure of phase transition.....	35
6-4. Converged potential energy, kinetic energy, non-bond energy and total energy.	36

1. Relationship of molecular structure-property

1-1. Detailed optimized gas-phase structures under M062x/6-311+G(d,p)

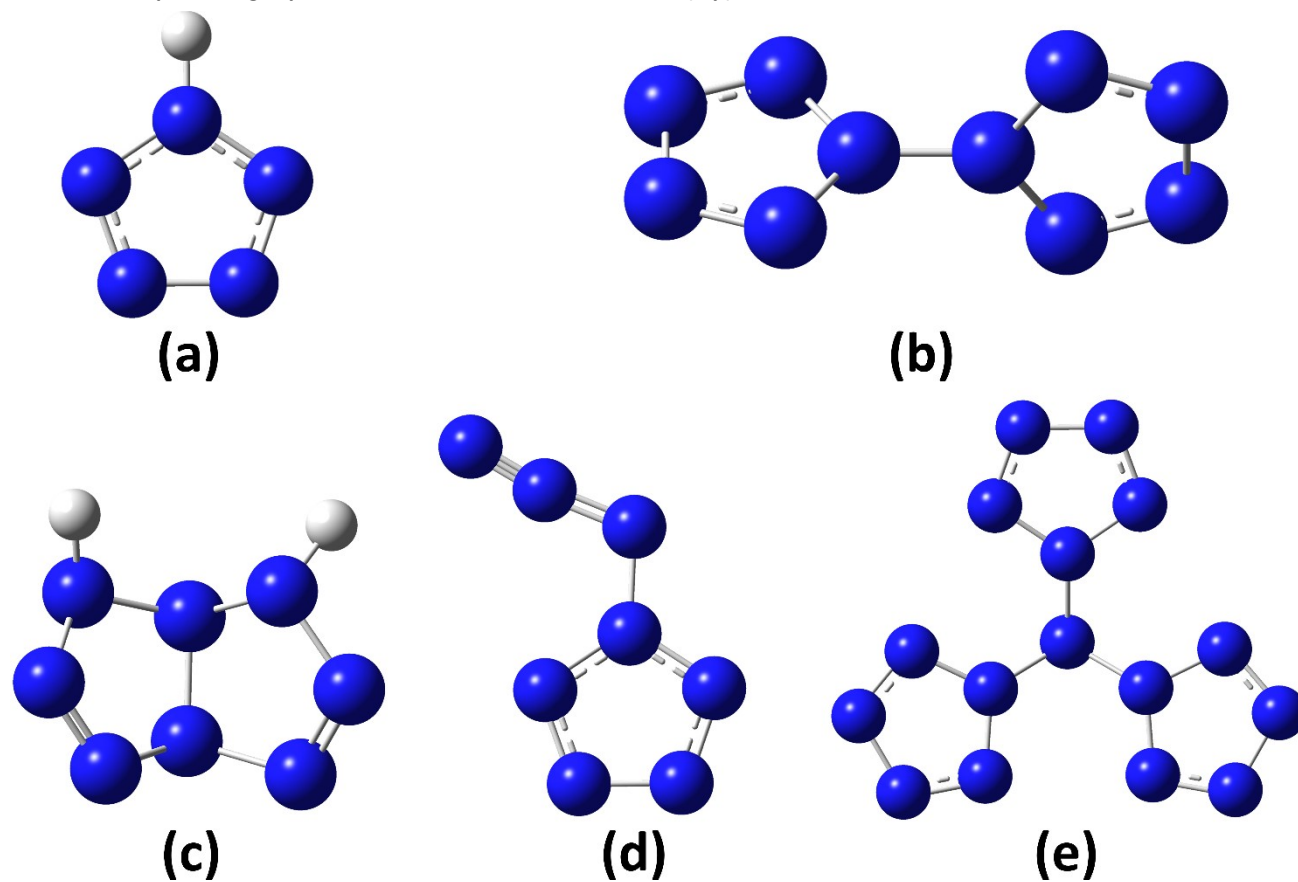


Fig S1. Optimized molecule structures of (a) pentazole (b) DPZ, (c) o-APN, (d) APZ and (e) t-PZA under the level of M062x/6-311+G(d,p).

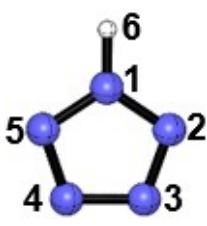
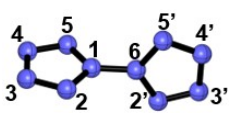
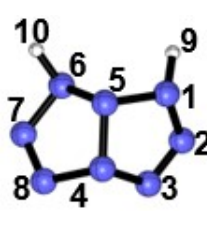
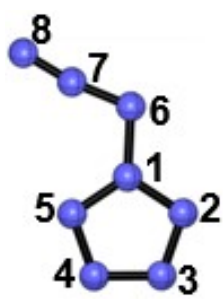

1-2. The vibrational frequencies of the four optimized gas-phase structures

Table S1. The vibrational frequencies of the four optimized monomer geometries.

Compounds	vibrational frequencies (cm ⁻¹)
DPZ	67.91, 125.96, 125.99, 449.47, 463.75, 463.86, 715.91, 716.05, 764.77, 788.22, 911.76, 930.80, 1094.49, 1094.74, 1137.61, 1159.81, 1211.72, 1215.56, 1216.42, 1331.49, 1376.71, 1519.58, 1519.88, 1594.31
o-APN	152.06, 296.08, 449.07, 551.29, 570.65, 651.21, 693.04, 718.43, 799.13, 819.90, 869.06, 914.07, 951.60, 999.23, 1034.84, 1085.91, 1130.82, 1158.84, 1396.75, 1437.97, 1674.90, 1719.34, 3557.97, 3588.40
APZ	22.41, 159.24, 285.80, 419.76, 498.04, 574.13, 709.38, 766.51, 828.39, 1043.96, 1109.91, 1179.58, 1219.22, 1241.19, 1301.90, 1447.86, 1479.69, 2342.17
t-PZA	32.99, 57.20, 57.84, 80.67, 81.46, 97.20, 201.06, 340.66, 341.26, 382.22, 421.81, 422.01, 657.58, 681.14, 711.50, 711.66, 774.89, 775.26, 776.34, 872.57, 873.11, 913.84, 962.88, 963.17, 1086.61, 1086.74, 1090.87, 1142.55, 1142.73, 1150.01, 1206.02, 1206.56, 1211.75, 1318.52, 1319.29, 1340.97, 1452.75, 1483.05, 1483.28, 1526.00, 1526.50, 1530.85

1-3. Optimized molecular structures with the typical bond length (Å), Wiberg bond index (WBI), Natural bond orbital charge (NBO), and bond angle (°).

Table S2 Optimized molecular structures of (a) N₅H, (b) DPZ, (c) o-APN, (d) APZ, (e) t-PZA with the typical bond length (Å), Wiberg bond index (WBI), Natural bond orbital charge (NBO), and bond angle (°). Blue: Nitrogen; White: Hydrogen.

N ₅ H	Bond Length (Å)/ Wiberg Index	NBO Charge (a.u.)	Bond Angle (°)				
	N1-N2	1.31/1.04	N1 -0.182	N1-N2-N3 104.60			
	N2-N3	1.29/1.10	N2 -0.041	N2-N3-N4 109.12			
	N3-N4	1.34/0.98	N3 -0.081	N3-N4-N5 109.12			
	N4-N5	1.29/1.10	N4 -0.081	N4-N5-N1 104.60			
	N5-N1	1.31/1.04	N5 -0.041	N2-N1-H6 123.72			
	N1-H6	1.01/0.71	H6 0.427				
	Bond Length (Å)/ Wiberg Index			NBO Charge (a.u.)		Bond Angle (°)	
	N1-N2	1.33/1.20	N1 0.086	N1-N2-N3 104.15			
	N2-N3	1.27/1.63	N2 0.007	N2-N3-N4 109.49			
	N3-N4	1.36/1.28	N3 -0.050	N3-N4-N5 109.45			
	N4-N5	1.27/1.63	N4 -0.051	N4-N5-N1 104.17			
	N5-N1	1.33/1.20	N5 0.007	N2-N1-N6 123.61			
	Bond Length (Å)/ Wiberg Index			NBO Charge (a.u.)		Bond Angle (°)	
	N1-N2	1.39/1.07	N1 -0.318	N1-N2-N3 110.58			
	N2-N3	1.22/1.93	N2 0.010	N2-N3-N4 108.51			
	N3-N4	1.48/0.95	N3 -0.022	N3-N4-N5 104.82			
	N4-N5	1.44/1.00	N4 -0.079	N4-N5-N1 99.11			
	N5-N1	1.42/1.02	N5 -0.031	N2-N1-H9 111.37			
	Bond Length (Å)/ Wiberg Index			NBO Charge (a.u.)		Bond Angle (°)	
	N1-N2	1.31/1.28	N1 -0.119	N1-N2-N3 103.98	109.47		
	N2-N3	1.30/1.51	N2 -0.036	N2-N3-N4 109.23			
	N3-N4	1.33/1.40	N3 -0.075	N3-N4-N5 104.01			
	N4-N5	1.29/1.50	N4 -0.067	N4-N5-N1 120.40			
	N5-N1	1.31/1.26	N5 -0.090	N2-N1-N6 109.81			
	N1-N6	1.38/1.01	N6 -0.185	N1-N6-N7 171.77			
	N6-N7	1.26/1.37	N7 0.235	N6-N7-N8			
	Bond Length (Å)/ Wiberg Index			NBO Charge (a.u.)		Bond Angle (°)	
	N1-N2	1.33/1.23	N1 -0.070	N1-N2-N3 104.43			
	N2-N3	1.28/1.59	N2 -0.009	N2-N3-N4 109.63			
	N3-N4	1.34/1.32	N3 -0.046	N3-N4-N5 109.63			
	N4-N5	1.28/1.59	N4 -0.046	N4-N5-N1 104.43			
	N5-N1	1.33/1.23	N5 -0.009	N2-N1-N6 122.81			
N1-N6	1.44/0.97	N6 0.119					

1-4. Molecular softness

The softness is derived from the concept density functional, which can reflect the degree of electron activity and distribution of deformation. Generally, the softer the molecule, the more likely to react.¹

$$Softness = \frac{1}{VIP - VEA} = \frac{1}{[E(N-1) - E(N)] - [E(N) - E(N+1)]} \quad (1)$$

The VIP is vertical ionization potential, VEA is vertical electron affinity, E is the electron energy, N is the number of electrons in the system, N+1 is the number of electrons after the system gained an extra electron, and n-1 is the number of electrons after it ionized an electron.

Table S3 The calculated different electron Energy (a.u.) and softness (1/a.u.) of the DPZ, o-APN, APZ, t-PZA.

molecule	E(N) (a.u.)	E(N-1) (a.u.)	E(N+1) (a.u.)	VIP (a.u.)	VEA (a.u.)	Softness(1/a.u.)
DPZ	-547.21	-546.74	-547.26	0.47	0.05	2.37
o-APN	-438.91	-438.49	-438.69	0.42	-0.22	1.55
APZ	-437.75	-437.34	-437.78	0.41	0.03	2.62
t-PZA	-875.46	-875.04	-875.47	0.42	0.01	2.46

2. Prediction of crystal structures based on Monte-Carlo method

2-1. Details of crystal structures predictions

The details are including four sections.

(1) Gas-phase calculation

First, we choose the optimized molecules in Figure S1(b)~(e) as the motion groups for packing the corresponding crystals. All the four molecules are optimized in Gaussian 16 package with the level of M06-2X/6-311+G(d,p).

(2) Definition of motion groups

Then we pack the molecule to obtain a crystal based on UFF forcefield. The optimized molecules are set as the motion groups, which are only allowed to rotate or translate as a rigid rotor in the packing process. All the intramolecular motions are forbidden in the heating and cooling processes. The motion groups are defined in the Figure S2.

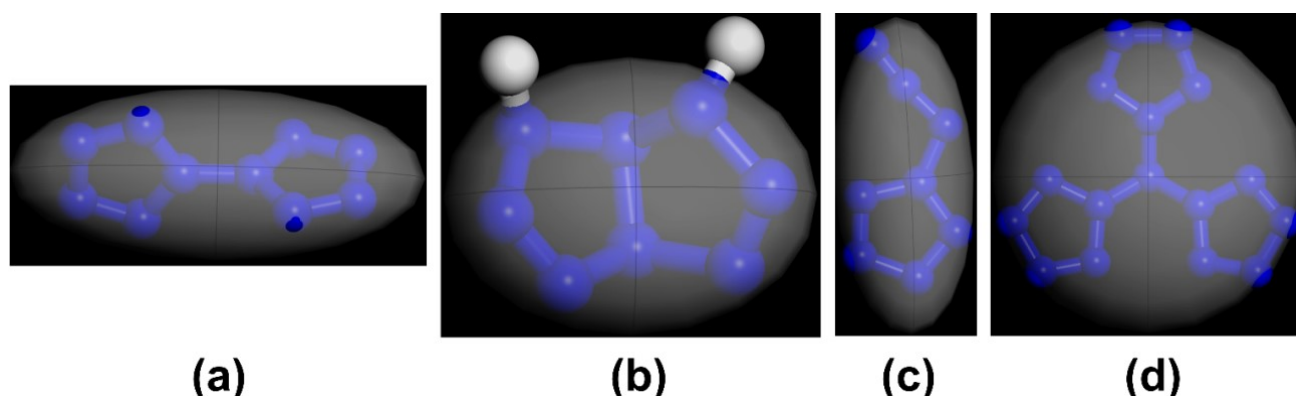


Fig S2. The defined motion group of the (a) DPZ, (b) o-APN, (c) APZ and (d) t-PZA.

(3) How MC works in Polymorph

As for the Monte Carlo methods in the package², the Packing phase with the space of possible crystal structures is searched for candidates of low energy. Here is the principle:

A crystal structure is specified by its crystal lattice parameters (cell lengths and angles) and the position and orientation of each molecule inside it. This yields a rugged energy landscape with many local minima, so a simulated annealing process is used. We provide the structure of the molecule of interest (or a structure containing multiple molecules), together with a force field (any of the usual force fields available in Materials Studio can be used). In addition, the space groups of interest must be provided (based on Belsky's theory in our study).

A trial MC move consists of reorienting and moving each molecule as a rigid body. Flexible molecules can also be handled: the user can specify which torsion angles are active, and these angles will also be changed during the MC procedure. Then, the size of the lattice cell is adjusted so that the molecules are just in contact but not overlapping. The energy is calculated, and the move is accepted or rejected according to the usual Metropolis criterion. The simulated annealing regime involves an initial heating phase, followed by cooling, and the whole process is repeated for each space group.

The set of structures generated by the Packing procedure can then be subjected to a Cluster analysis, which reduces it by removing similar structures. The criterion for similarity is based on the radial distribution function; a similarity measure is calculated from the difference between the radial distribution functions of the two structures, and if this lies within a specified tolerance, the structures are deemed to be similar, and the one of highest energy is eliminated. The candidate structures are usually optimized at this point and again passed through the Cluster analysis. Finally, they are ranked in order of energy. This is the output from Polymorph Predictor.

(4) What we have done in the prediction

Here we apply the Monte-Carlo algorithm by Polymorph code² for our prediction. The determination of space groups is based on the principle pointed out by Belsky,³ where 88.6% of the organic molecular crystal structures belonged to the following space groups: $P2_1/c$, $P2_12_12_1$, $P1$, $P2_1$, $C2/c$, $Pbca$, $Pna2_1$, $Pnma$, $Pbcn$.

MC packing algorithm follows a simulated annealing procedure intended to search for the lowest minima of the energy function G of molecular crystals, where G decomposes as $G = E + pV - TS$ in the thermodynamics states. In Polymorph code, TS can be neglected because this factor changes the calculated energy slightly based on the known value of G . It should be noticed the predicted structures with lowest energy should represent experimental results but with different stabilities. And the electronic energy E is efficiently computed by using a UFF forcefield.⁴ The first step of a polymorph prediction sequence is a MC packing simulation to search for the global minimum of each selected space group. The simulation consists of two phases, heating and cooling. First, each trial crystal is heated. During heating, one starts from a set minimum temperature (300 K in our case). Each new trial temperature T_{new} is obtained using Eq. 2, where T_{old} is the temperature used in a previous step and T_h is a heating factor (1 in our case). Heating continues until either a pre-set maximum temperature is reached (3×10^5 K in our case) or a specified number of consecutive trial moves have been accepted.

$$T_{new} = T_{old} \times (1.0 + T_h) \quad (2)$$

The cooling phase simulates the annealing of a heated structure. At high temperatures the algorithm is able to globally sample the phase space of possible packing arrangements. At low temperatures the algorithm samples areas of energetically favorable packing arrangements more locally. If a trial is accepted during cooling, the temperature to be used in the next trial step, T_{new} , is obtained using Eq.3, where T_{old} is the temperature used in a previous step and T_c is a user-definable cooling factor (0.0005 in our case).

$$T_{new} = T_{old} \times (1.0 - T_c) \quad (3)$$

The simulation ends when T is so low that the crystal is frozen (300 K in our case). Then one can optimize at 300 K all the found structures during the annealing procedure and determine the structure with the lowest energy.

(5) The comparisons of MC predictions and experimental results

In our manuscript, all the molecules can be seen as organic rigid CHN(O) systems. To make sure our results reliable, we have compared our predictions based on the Belsky's theory with the already known crystal structures of tetrazole series systems, including 1H-tetrazole⁵ (CCDC: 128628) and 5-amino-tetrazole⁶ (CCDC: 790420). For 1H-tetrazole, the predicted crystal structures with P_1 space group appears the lowest potential energy, which is fully consistent with the experimental result as the Table S4. For 5-amino-tetrazole, the predicted $P2_12_12_1$ -crystal is also show consistence with the experimental results.

Table S4 The lowest total energy (kcal/mol), Van der Waals (vdW) energy (kcal/mol), the number of predicted structures and crystal parameters of the 1H-tetrazole and 5-amino-tetrazole by applied MC methods and the comparison of experimental results.

1H-tetrazole				
Experimental results: $P1$; $a=3.73$, $b=4.77$, $c=4.94$; $\alpha=107.03$, $\beta=107.23$, $\gamma=101.57$.				
Space group	total energy (kcal/mol)	Van der Waals energy (kcal/mol)	Number of predicted structures	Crystal parameters
$C2/c$	-4.01	-7.28	104	$a=19.04$, $b=6.47$, $c=5.72$; $\alpha=90.00$, $\beta=70.75$, $\gamma=90.00$.
$P1$	-4.33	-7.61	909	$a=3.66$, $b=6.61$, $c=5.21$; $\alpha=129.94$, $\beta=110.90$, $\gamma=93.81$.
$P2_1$	-4.23	-7.51	1526	$a=6.10$, $b=8.23$, $c=3.64$; $\alpha=90.00$, $\beta=63.56$, $\gamma=90.00$.
$P2_1/c$	-4.29	-7.57	1144	$a=5.25$, $b=12.92$, $c=5.68$; $\alpha=90.00$, $\beta=57.81$, $\gamma=90.00$.
$P2_12_12_1$	-3.25	-6.74	43	$a=3.59$, $b=9.70$, $c=9.45$; $\alpha=90.00$, $\beta=90.00$, $\gamma=90.00$.
$Pbca$	-3.17	-6.68	859	$a=19.17$, $b=3.64$, $c=9.49$; $\alpha=90.00$, $\beta=90.00$, $\gamma=90.00$.

<i>Pbcn</i>	-3.16	-6.65	653	a=19.15, b=5.13, c=6.74; α=90.00, β=90.00, γ=90.00.
<i>Pna2₁</i>	-3.24	-6.74	2727	a=9.43, b=9.72, c=3.59; α=90.00, β=90.00, γ=90.00.
<i>Pnma</i>	-2.76	-6.25	419	a=9.56, b=19.49, c=3.69; α=90.00, β=90.00, γ=90.00.

5-amino-tetrazole

Experimental results: *P2₁2₁2₁*; a=4.96, b=3.26, c=17.54; α=90.00, β=90.00, γ=90.00.

Space group	total energy (kcal/mol)	Van der Waals energy (kcal/mol)	Number of predicted structures	Crystal parameters
<i>C2/c</i>	36.20	-9.63	392	a=12.63, b=3.43, c=17.78; α=90.00, β=96.84, γ=90.00.
<i>P1</i>	36.62	-9.21	3181	a=5.24, b=3.40, c=16.34; α=90.00, β=111.65, γ=108.91.
<i>P2₁</i>	36.22	-9.61	2790	a=8.25, b=3.41, c=6.91; α=90.00, β=80.82, γ=90.00.
<i>P2₁/c</i>	36.18	-9.70	533	a=3.45, b=15.92, c=7.62; α=90.00, β=114.70, γ=90.00.
<i>P2₁2₁2₁</i>	36.15	-9.73	1124	a=6.93, b=3.41, c=16.14; α=90.00, β=90.00, γ=90.00.
<i>Pbca</i>	36.25	-9.58	64	a=8.89, b=6.85, c=12.62; α=90.00, β=90.00, γ=90.00.
<i>Pbcn</i>	36.33	-9.51	370	a=8.90, b=6.86, c=12.66; α=90.00, β=90.00, γ=90.00.
<i>Pna2₁</i>	36.17	-9.68	3666	a=16.14, b=6.93, c=3.41; α=90.00, β=90.00, γ=90.00.
<i>Pnma</i>	37.05	-8.77	2124	a=7.01, b=24.62, c=4.84; α=90.00, β=90.00, γ=90.00.

(6) The predictions of the four pentazole complexes

The minimum energy and cell parameters corresponding to the crystal structures of the four pentazole are shown in Table S5. The predicted crystal structures are showed in Fig. S3.

Table S5 The lowest Gibbs free energy (kcal/mol), vDW energy (kcal/mol), density (g/cm³) and crystal parameters of the predicted structures with different space groups.

Space group	total energy (lowest)	Van der Waals energy	Density	Number of predicted structures	Crystal parameters
<i>C2/c</i>	-3.03	-7.28	1.75	91	a=30.88, b=3.54, c=9.74; α=90.00, β=92.38, γ=90.00.
<i>P1</i>	-3.11	-7.34	1.76	3513	a=8.48, b=3.53, c=7.08; α=43.57, β=91.29, γ=74.08.
<i>P2₁</i>	-3.13	-7.35	1.78	3689	a=5.31, b=5.06, c=9.75; α=90.00, β=85.76, γ=90.00.
<i>P2₁/c</i>	-3.14	-7.36	1.78	3325	a=5.05, b=11.44, c=10.36;

Space group	Total energy (lowest)	Vander Waal's Energy	Density	Number of predicted structures	Crystal parameters
<i>P2₁2₁2₁</i>	-3.13	-7.36	1.78	338	$\alpha=90.00, \beta=60.80, \gamma=90.00$ a=11.44, b=5.05, c=9.04; $\alpha=90.00, \beta=90.00, \gamma=90.00$.
<i>Pbca</i>	-3.02	-7.26	1.75	926	a=16.30, b=9.24, c=7.08; $\alpha=90.00, \beta=90.00, \gamma=90.00$.
<i>Pbcn</i>	-2.79	-7.02	1.75	312	a=4.91, b=11.68, c=18.57; $\alpha=90.00, \beta=90.00, \gamma=90.00$.
<i>Pna2₁</i>	-3.12	-7.36	1.78	2750	a=11.44, b=5.05, c=9.04; $\alpha=90.00, \beta=90.00, \gamma=90.00$.
<i>Pnma</i>	-2.42	-6.66	1.65	983	a=9.70, b=32.86, c=3.53; $\alpha=90.00, \beta=90.00, \gamma=90.00$.

o-APN

Space group	Total energy (lowest)	Vander Waal's Energy	Density	Number of predicted structures	Crystal parameters
<i>C2/c</i>	-3.04	-7.50	1.72	1713	a=11.60, b=5.58, c=13.93; $\alpha=90.00, \beta=77.52, \gamma=90.00$.
<i>P1</i>	-2.46	-6.96	1.66	962	a=9.13, b=9.99, c=5.57; $\alpha=57.98, \beta=136.94, \gamma=157.10$.
<i>P2₁</i>	-2.81	-7.21	1.70	1668	a=6.39, b=7.03, c=6.43; $\alpha=90.00, \beta=129.46, \gamma=90.00$.
<i>P2₁/c</i>	-2.97	-7.43	1.71	1292	a=6.55, b=13.30, c=5.72; $\alpha=90.00, \beta=117.41, \gamma=90.00$.
<i>P2₁2₁2₁</i>	-2.75	-7.22	1.69	543	a=6.50, b=8.89, c=7.75; $\alpha=90.00, \beta=90.00, \gamma=90.00$.
<i>Pbca</i>	-2.78	-7.26	1.70	63	a=7.19, b=12.41, c=10.00; $\alpha=90.00, \beta=90.00, \gamma=90.00$.
<i>Pbcn</i>	-2.87	-7.35	1.70	213	a=7.34, b=12.28, c=9.89; $\alpha=90.00, \beta=90.00, \gamma=90.00$.
<i>Pna2₁</i>	-2.67	-7.15	1.69	2094	a=9.91, b=4.08, c=11.10; $\alpha=90.00, \beta=90.00, \gamma=90.00$.
<i>Pnma</i>	-1.69	-6.14	1.58	1933	a=10.11, b=17.07, c=5.56; $\alpha=90.00, \beta=90.00, \gamma=90.00$.

APZ

Space group	Total energy (lowest)	Vander Waal's Energy	Density	Number of predicted structures	Crystal parameters
<i>C2/c</i>	-5.76	-8.06	1.60	1032	a=16.20, b=8.74, c=6.67; $\alpha=90.00, \beta=80.36, \gamma=90.00$.
<i>P1</i>	-5.25	-7.53	1.55	2731	a=6.91, b=5.13, c=3.72; $\alpha=74.11, \beta=107.57, \gamma=88.45$.
<i>P2₁</i>	-5.60	-7.93	1.60	3271	a=8.69, b=4.04, c=7.69; $\alpha=90.00, \beta=120.71, \gamma=90.00$.
<i>P2₁/c</i>	-5.78	-8.09	1.62	1913	a=3.90, b=14.82, c=9.22; $\alpha=90.00, \beta=59.71, \gamma=90.00$.
<i>P2₁2₁2₁</i>	-5.62	-7.92	1.61	1346	a=8.80, b=13.03, c=4.02;

<i>Pbca</i>	-5.72	-8.02	1.60	2846	$\alpha=90.00, \beta=90.00, \gamma=90.00.$ a=15.99, b=8.66, c=6.72; $\alpha=90.00, \beta=90.00, \gamma=90.00.$
<i>Pbcn</i>	-5.41	-7.75	1.56	80	a=16.10, b=8.76, c=6.77; $\alpha=90.00, \beta=90.00, \gamma=90.00.$
<i>Pna2₁</i>	-5.63	-7.90	1.59	20	a=15.94, b=7.86, c=3.74; $\alpha=90.00, \beta=90.00, \gamma=90.00.$
<i>Pnma</i>	-5.13	-7.46	1.48	1257	a=6.67, b=17.44, c=8.62; $\alpha=90.00, \beta=90.00, \gamma=90.00.$

t-PZA

Space group	Total energy (lowest)	Vander Waal's Energy	Density	Number of predicted structures	Crystal parameters
<i>C2/c</i>	12.68	0.20	1.78	1482	a=14.00, b=9.68, c=14.11; $\alpha=90.00, \beta=60.78, \gamma=90.00.$
<i>P1</i>	13.94	1.39	1.70	737	a=8.18, b=4.43, c=7.78; $\alpha=88.45, \beta=67.19, \gamma=59.49.$
<i>P2₁</i>	12.77	0.23	1.78	1628	a=8.63, b=10.77, c=4.66; $\alpha=90.00, \beta=74.43, \gamma=90.00.$
<i>P2₁/c</i>	12.61	0.07	1.80	1184	a=7.64, b=8.41, c=14.85; $\alpha=90.00, \beta=119.92, \gamma=90.00.$
<i>P2₁2₁2₁</i>	12.69	0.11	1.80	863	a=12.94, b=8.51, c=7.52; $\alpha=90.00, \beta=90.00, \gamma=90.00.$
<i>Pbca</i>	13.11	0.56	1.77	460	a=12.00, b=9.60, c=14.62; $\alpha=90.00, \beta=90.00, \gamma=90.00.$
<i>Pbcn</i>	13.33	0.68	1.70	157	a=9.87, b=13.95, c=12.34; $\alpha=90.00, \beta=90.00, \gamma=90.00.$
<i>Pna2₁</i>	12.78	1.18	1.72	692	a=8.18, b=13.42, c=7.87; $\alpha=90.00, \beta=90.00, \gamma=90.00.$
<i>Pnma</i>	14.48	1.82	1.59	398	a=6.92, b=25.98, c=10.40; $\alpha=90.00, \beta=90.00, \gamma=90.00.$

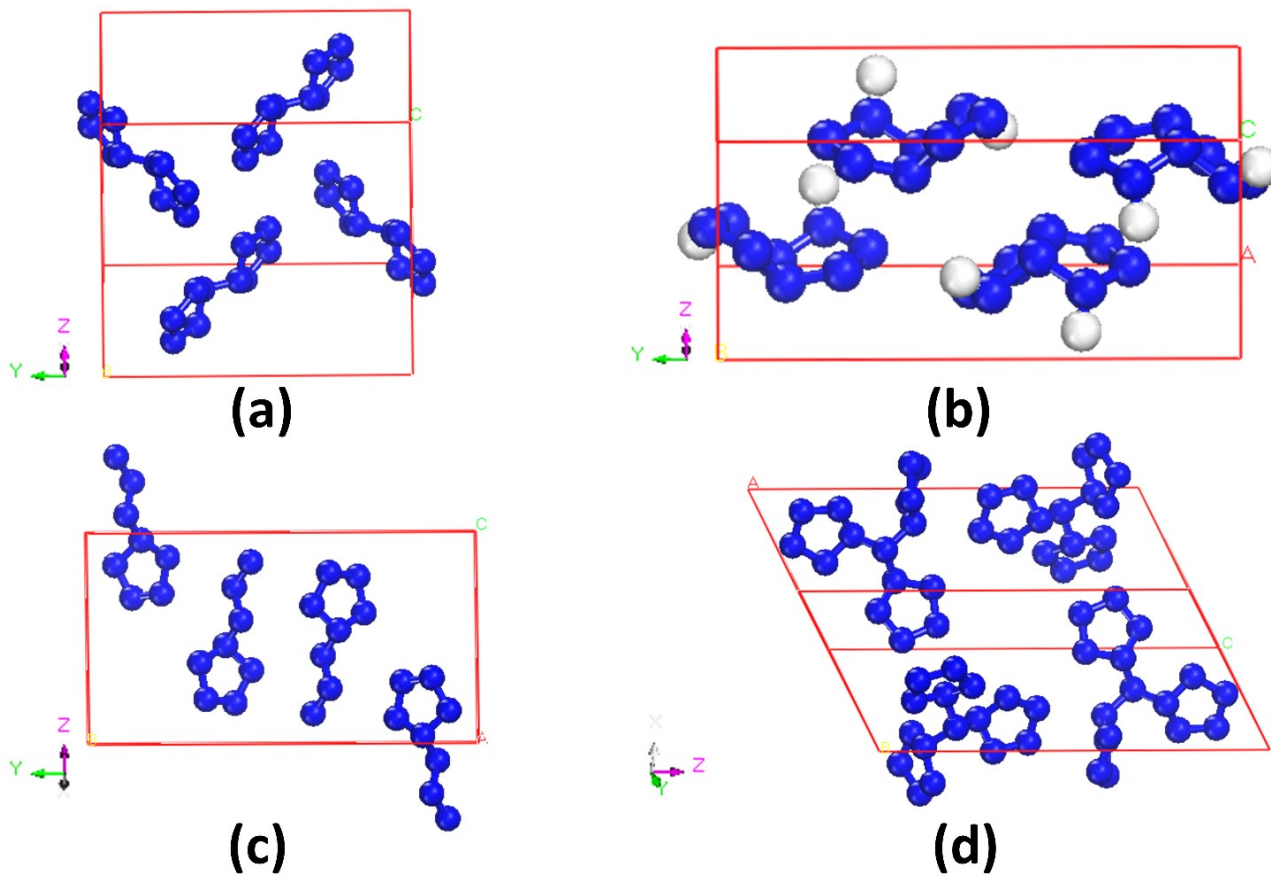


Fig S3. The four predicted crystal structures. (a) DPZ, (b) o-APN, (c) APZ, (d) t-PZA.

2-2. The benchmark calculation of the different Forcefield.

UFF⁴ as a molecular mechanics force field is a full periodic table force field, which is broadly applied in structural predictions and MD/MM simulations. To confirm UFF is an acceptable force field in the limited time, we compare the predictions with COMPASS FF⁷ (ab Initio FF) and Dreiding FF⁸ (a generic FF). The space group has been limited as P_1 and $P2_12_12_1$ for 1H-tetrazole and 5-amino-tetrazole, respectively. The parameters, lowest total energies, vdW energies and Number of predicted structures are summarized in the Table S6. Based on the comparison, UFF is not only providing acceptable predicted results, but also spending the shortest time in the prediction. As a full periodic table forcefield, the UFF results can be applied to compare with each other conveniently in the future.

Table S6 The comparison of UFF, COMPASS FF and Dreiding FF for predicting the P_1 -1H-tetrazole and $P2_12_12_1$ -5-amino-tetrazole.

1H-tetrazole	Total energy (lowest)	Vander Waal's Energy	Number of predicted structures	Crystal parameters	Time spending (s)
UFF	-4.33	-7.41	2230	a=3.66, b=6.61, c=5.21; $\alpha=129.94$, $\beta=110.90$, $\gamma=93.81$.	538
COMPASS FF	193.93	-8.32	3938	a=4.84, b=3.60, c=5.57; $\alpha=107.06$, $\beta=60.20$, $\gamma=86.38$.	1340
Dreiding FF	-3.46	-5.63	1887	a=5.37, b=4.55, c=5.88; $\alpha=104.14$, $\beta=123.65$, $\gamma=115.66$.	572
Exp	--	--	--	a=3.73, b=4.77, c=4.94; $\alpha=107.03$, $\beta=107.23$, $\gamma=101.57$.	--
5-amino-tetrazole	Total energy (lowest)	Vander Waal's Energy	Number of predicted structures	Crystal parameters	Time spending (s)
UFF	-36.15	-9.68	2540	a=6.93, b=3.41, c=16.14; $\alpha=90.00$, $\beta=90.00$, $\gamma=90.00$.	667
COMPASS FF	-27.29	-12.79	3782	a=6.68, b=7.53, c=6.63; $\alpha=90.00$, $\beta=90.00$, $\gamma=90.00$.	1355
Dreiding FF	-0.53	-3.67	2410	a=8.79, b=3.86, c=10.38; $\alpha=90.00$, $\beta=90.00$, $\gamma=90.00$.	824
Exp	--	--	--	a=4.96, b=3.26, c=17.54; $\alpha=90.00$, $\beta=90.00$, $\gamma=90.00$.	--

3. Crystal structures

3-1. Test for the convergence criteria in crystal optimization

We have done a benchmark for comparing the structure of 1H-tetrazole. With the method of GGA-PBE (Grimme-D3), the threshold applied in the manuscript including: Energy < 5×10^{-6} eV/atom, residual forces < 0.01 eV/Å, residual stress < 0.02 GPa and Max displacement < 5×10^{-4} Å, respectively. The Monkhorst-pack grid for k-points is $3 \times 2 \times 2$ with the cut-off energy of 500 eV.

Then we compare cell parameters and total energies calculated by stricter criteria and more loose criteria in both CASTEP and VASP package.

Stricter criteria: Energy < 1×10^{-6} eV/atom, residual forces < 0.005 eV/Å, residual stress < 0.01 GPa and Max displacement < 1×10^{-4} Å.

Loose criteria: Energy < 1×10^{-5} eV/atom, residual forces < 0.02 eV/Å, residual stress < 0.04 GPa and Max displacement < 1×10^{-3} Å

Table S7 The results of the convergence test.

1H-tetrazole (CASTEP)	Cell parameters	Energy (eV)	Time (s)
Higher	a=3.657, b=4.672, c=4.851; $\alpha=106.59$, $\beta=107.45$, $\gamma=99.19$	-1270.202	1256
Applied in our calculation	a=3.622, b=4.686, c=4.848; $\alpha=106.94$, $\beta=107.23$, $\gamma=99.08$	-1270.196	292
Lower	a=3.657, b=4.678, c=4.850; $\alpha=106.53$, $\beta=107.47$, $\gamma=99.24$	-1270.197	98
Experimental results	a=3.725, b=4.773, c=4.936; $\alpha=107.03$, $\beta=107.23$, $\gamma=101.57$	--	--

3-2. k-point test and cut-off test

The k-point test (with the cutoff energy of 500 eV) and cut-off test (with the k-points grid of 3×1×2、1×2×1、4×1×2 and 2×2×1 Monkhorst–Pack meshes) are summarized below. Based on the tests, The k-point grid of 3×1×2、1×2×1、4×1×2 and 2×2×1 Monkhorst–Pack meshes³⁶ are used to describe the Brillouin-zones for DPZ, o-APN, APZ and t-PZA, respectively.

Table S8 The tests of k-point grids and cutoff energy of DPZ.

DPZ		
K points (Monkhorst-pack grid)	Energy (eV)	Time (s)
1×1×1	-10797.70	50.06
2×1×2	-10796.78	239.50
3×1×2	-10797.79	352.36
3×1×3	-10797.79	419.27
4×2×2	-10796.80	347.97
Cutoff energy	Energy (eV)	Time (s)
300	-10795.86	173.81
400	-10796.39	293.41
500	-10797.79	352.36
600	-10796.85	442.23
700	-10797.02	602.94

Table S9 The tests of k-point grids and cutoff energy of o-APN.

o-APN		
K points (Monkhorst-pack grid)	Energy (eV)	Time (s)
1×1×1	-17531.46	391.61
1×2×1	-17532.78	936.73
1×3×1	-17532.77	2745.78
1×2×2	-17532.78	1084.58
2×2×1	-17532.78	1030.36
Cutoff energy	Energy (eV)	Time (s)
300	-17529.65	920.40
400	-17530.78	1656.14
500	-17532.78	936.73
600	-17531.58	3397.58
700	-17531.91	3798.61

Table S10 The tests of k-point grids and cutoff energy of APZ.

APZ		
K points (Monkhorst-pack grid)	Energy (eV)	Time (s)
1×1×1	-8624.16	692.56
2×1×1	-8627.30	294.98
3×1×2	-8627.35	2440.75
4×1×2	-8627.37	2087.02
5×1×2	-8627.34	2376.69
Cutoff energy	Energy (eV)	Time (s)
300	-8626.63	655.77
400	-8627.03	963.09
500	-8627.37	2087.02
600	-8627.33	2111.06
700	-8627.30	2350.41

Table S11 The tests of k-point grids and cutoff energy of t-PZA.

t-PZA		
K points (Monkhorst-pack grid)	Energy (eV)	Time (s)
1×1×1	-17273.17	787.59
2×1×1	-17273.09	1499.14
1×2×1	-17273.18	1430.50
2×2×1	-17273.24	1522.92
3×2×1	-17273.16	1902.62
Cutoff energy	Energy (eV)	Time (s)
300	-17271.66	586.86
400	-17272.50	915.64
500	-17273.24	1522.92
600	-17273.23	1340.55
700	-17273.22	1555.58

3-3. Optimized crystal structures of pentazole derivate compounds

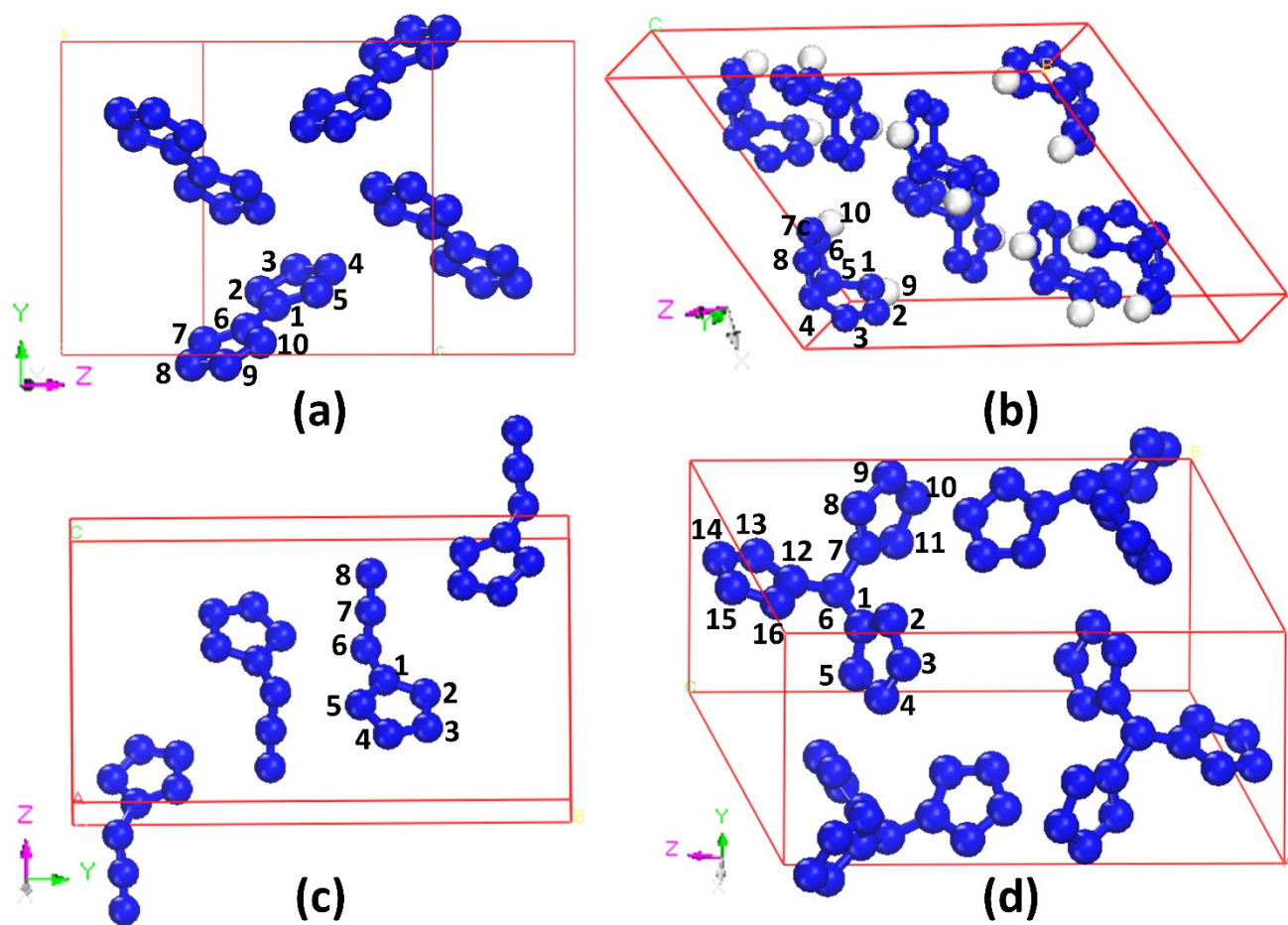


Fig S4. The four optimized crystal structures. (a) DPZ, (b) o-APN, (c) APZ, (d) t-PZA.

Table S12. The optimized theoretical cell parameters and atomic coordinates of DPZ.

DPZ			
Crystallographic system	Monoclinic		
Symmetry group	$P2_1/c$		
a	6.11471	α	90.0000
b	9.26732	β	56.7917
c	11.1678	γ	90.0000
atom coordination			
N1	0.845690	0.158029	0.250012
N2	1.06928	0.200027	0.128157
N3	1.19336	0.270983	0.176495
N4	1.04591	0.271188	0.323643
N5	0.825023	0.200368	0.371915
N6	0.651907	0.0818952	0.249962
N7	0.673039	0.0391490	0.128076
N8	0.453135	-0.0327004	0.176317
N9	0.305667	-0.0325227	0.323532
N10	0.428881	0.0394394	0.371817

Table S13. The optimized theoretical cell parameters and atomic coordinates of o-APN.

o-APN			
Crystallographic system	Monoclinic		
Symmetry group	$C2/c$		
a	11.6385	α	90.0000
b	4.97923	β	120.795
c	16.0806	γ	90.0000
atom coordination			
N1	0.878139	0.424308	0.852441
N2	0.928540	0.650663	0.839560
N3	0.913973	0.854314	0.882533
N4	0.847501	0.766553	0.935107
N5	0.848389	0.468652	0.932004
N6	0.710275	0.416096	0.900086
N7	0.632445	0.633016	0.856559
N8	0.703612	0.844792	0.874165
H9	0.926936	0.242229	0.859567
H10	0.675987	0.222068	0.874268

Table S14. The optimized theoretical cell parameters and atomic coordinates of APZ.

APZ			
Crystallographic system	Monoclinic		
Symmetry group	$P2_1/c$		
a	3.68710	α	90.0000
b	15.5572	β	59.0199
c	9.41386	γ	90.0000
atom coordination			
N1	0.793768	0.627232	0.441085
N2	0.802787	0.709147	0.390809
N3	1.15674	0.713470	0.244951
N4	1.35530	0.634957	0.206387
N5	1.12836	0.580190	0.328105
N6	0.446016	0.590974	0.579499
N7	0.455772	0.601356	0.712843
N8	0.388704	0.602141	0.849177

Table S15. The optimized theoretical cell parameters and atomic coordinates of t-PZA.

t-PZA			
Crystallographic system	Monoclinic		
Symmetry group	$P2_1/c$		
a	7.04600	α	90.0000
b	9.38147	β	111.469
c	13.8598	γ	90.0000
atom coordination			
N1	0.304066	0.506937	0.713626
N2	0.397614	0.605382	0.674482
N3	0.567881	0.541570	0.680695
N4	0.578630	0.408448	0.725445
N5	0.412546	0.385358	0.745495
N6	0.121204	0.527791	0.729421
N7	-0.0196348	0.606731	0.648773
N8	-0.0584733	0.747720	0.651621
N9	-0.206988	0.770894	0.561848
N10	-0.253260	0.646140	0.505560
N11	-0.138873	0.541632	0.560609
N12	0.157300	0.591624	0.827055
N13	0.0123121	0.597723	0.868997
N14	0.109231	0.657330	0.960617
N15	0.309335	0.681595	0.973660
N16	0.341282	0.641727	0.889321

3-4. Lattice energy

The theoretically calculated lattice energy is used to analyze the stability of the four crystals from the perspective of energetics. Lattice energy (LE) is defined as the total energy difference between the crystal in the free state and the constituent ions in the free state, as shown in formula 3, where the n is the number of the molecules in the crystal.

$$LE = \frac{1}{n} E_{crystal}^{total} - E_{molecule}^{total} \quad (3)$$

In order to avoid the influence of the interaction on the lattice energy, we calculate the energy of a molecule in the crystal under vacuum, which is -2701.62377 eV of the DPZ, -2192.71265 eV of the o-APN, -2160.87426 eV of the APZ, and -4322.27342 eV of the t-PZA, respectively. The smaller the value of the lattice energy, the more stable the crystal is.

Table S16. The calculated Lattice Energy (eV) of the DPZ, o-APN, APZ, t-PZA at the different pressures.

Lattice Energy (eV)	DPZ	o-APN	APZ	t-PZA
0GPa	-0.54	-1.08	-0.41	-0.68
20GPa	11.74	8.78	9.76	19.35
40GPa	21.66	16.86	17.79	34.63
60GPa	30.54	24.17	23.50	48.74
80GPa	38.75	30.94	29.85	63.01
100GPa	46.46	37.63	36.95	75.24
120GPa	53.40	43.36	42.48	86.72
140GPa	60.33	49.29	47.00	97.64
160GPa	66.48	54.69	52.21	108.10
180GPa	73.27	59.97	57.26	117.90
200GPa	79.21	65.19	62.15	126.43

3-5. Phonon calculation

The same parameters in the optimization have been chosen for the original structure for the phonon calculation. The phonon calculation has been explored with a finite displacement calculation which proceeds by shifting each atom by a small amount, then performing a Self-Consistent Field calculation to evaluate the forces on the perturbed configuration. The cutoff radius of the cell for each crystal has been set as 4 Å. The set of k points have been chosen at Γ point.

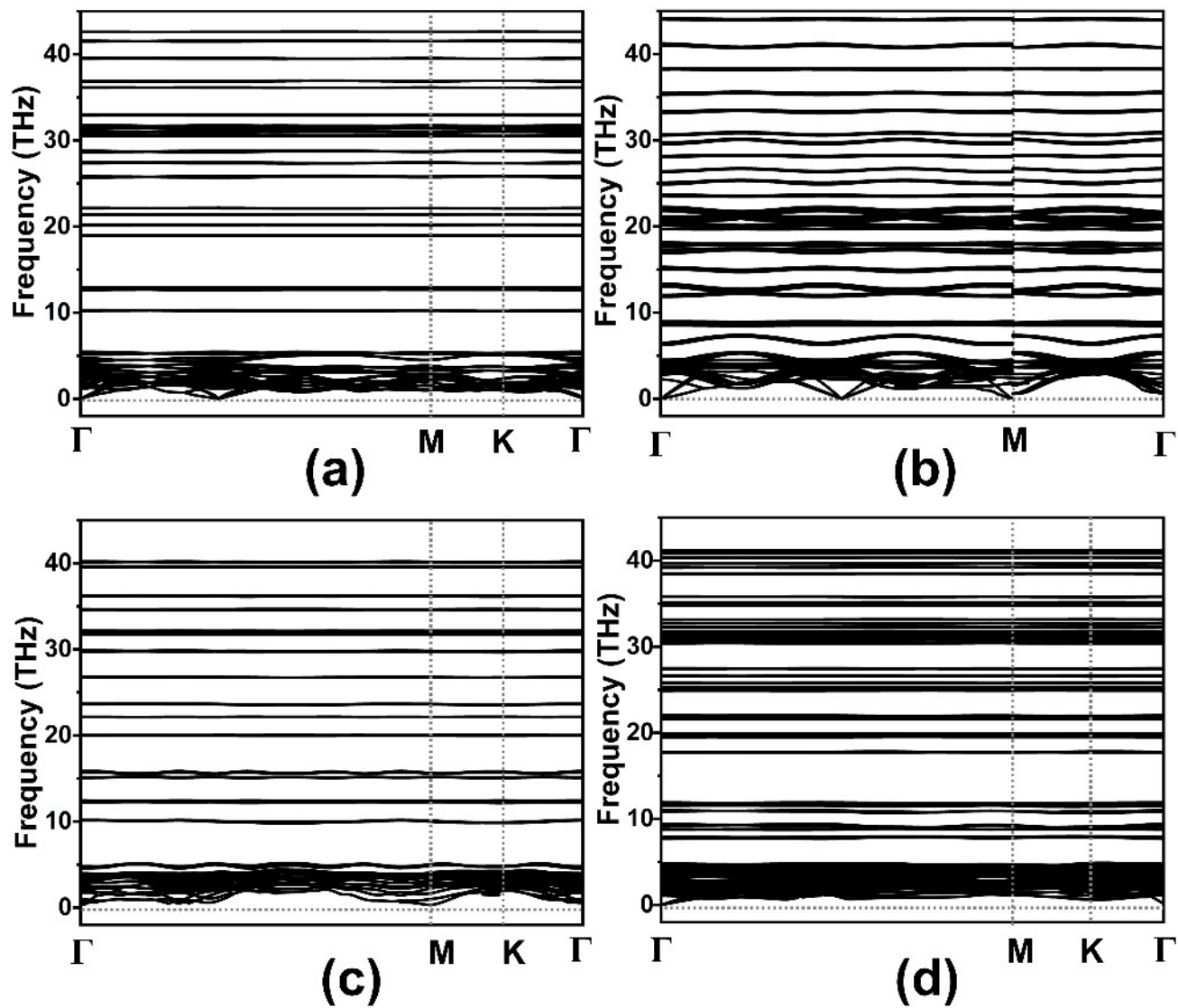


Fig. S5 Phonon spectra of the crystal structures. (a) DPZ, (b) o-APN, (c) APZ, (d) t-PZA.

4. Formation enthalpy

4-1. Formation of enthalpy of gas phase

In our calculation, the condensed-phase enthalpy of formation can be obtained by the gas-phase heats of formation and enthalpy of sublimation according to Hess' law in equation (4):

$$\Delta_f H (\text{Solid}) = \Delta_f H (\text{Gas}) - \Delta H (\text{Sublimation}) \quad (4)$$

where $\Delta H (\text{Gas})$ is obtained by calculating the atomization reaction energy using the known heat of formation of isolated atoms.

The atomization equation of molecule $A_x B_y C_z$ is as: $A_x B_y C_z \rightarrow xA + yB + zC$

$$\Delta_r H_{298K} = x\Delta_f H_{298K}(A) + y\Delta_f H_{298K}(B) + z\Delta_f H_{298K}(C) - \Delta_f H_{298K}(A_x B_y C_z) \quad (5)$$

$$\Delta_r H_{298K} = \Delta E_0 + \Delta H_T \quad (6)$$

In the equation, $\Delta_f H_{298K}(A)$, $\Delta_f H_{298K}(B)$, $\Delta_f H_{298K}(C)$, $\Delta_f H_{298K}(A_x B_y C_z)$ are the enthalpy of formation of atoms A, B, C and molecules $A_x B_y C_z$ at 298K, respectively. ΔH_T is the corrected enthalpy triggered by different temperature.

Table S17 The calculated E_0 (a.u), ΔH_T (kJ/mol), $\Delta_f H_{298K}$ (kJ/mol) of the DPZ, o-APN, APZ, t-PZA.

Atom/molecule	E_0 (a.u)	ΔH_T (kJ/mol)	$\Delta_f H_{298K}$ (kJ/mol)
N	-54.584622	4.35344	471.05 ⁹
H	-0.498134	4.22786	216.12 ⁹
pentazole	-274.198073	11.02186	545.81
DPZ	-547.160951	19.35656	1281.21
o-APN	-438.851432	16.52229	1132.60
APZ	-437.715417	15.62131	1059.88
t-PZA	-875.377477	25.16168	2266.00

4-2. The sublimation enthalpies of condensed-phase

1. DFT calculation

The heats of sublimation can be represented as the formula (7) based on the optimized gas-phase and solid structures with the method of GGA-PBE. The gas-phase structures are optimized under the level of PBE/6-311+G(d,p) in Gaussian.

$$\Delta_{\text{sub}} H = -E_{\text{coh}}^{\text{cr}} + \Delta_{\text{geom}}^{\text{cr} \rightarrow \text{g}} E + \Delta_{\text{ZPE}}^{\text{cr} \rightarrow \text{g}} E + \Delta_{\text{th,mol}}^{\text{cr} \rightarrow \text{g}} E + H_{\text{th,mol}}^{\text{lattice}} + H_{\text{ro-tr}}^{\text{g}} \quad (7)$$

$E_{\text{coh}}^{\text{cr}}$ is the cohesive energy, which is defined as the total energy difference between the crystal and the optimized molecules, as shown in formula (3), where the n is the number of the molecules in the crystal. In the calculation, we have built $30 \times 30 \times 30 \text{ \AA}$ box for calculating the total energy of molecules. $\Delta_{\text{geom}}^{\text{cr} \rightarrow \text{g}} E$ represents the energy change associated with the relaxation of a molecule in its crystal phase geometry to the geometry of an isolated molecule in the vapor phase. $\Delta_{\text{ZPE}}^{\text{cr} \rightarrow \text{g}} E$ and $\Delta_{\text{th,mol}}^{\text{cr} \rightarrow \text{g}} E$ represent the energy differences between the gas phase and crystal phase zero-point vibration energy and intramolecular contributions to thermal enthalpy, respectively. $H_{\text{th,mol}}^{\text{lattice}}$ and $H_{\text{ro-tr}}^{\text{g}}$ are implicitly included in the calculated enthalpies of both phases¹⁰.

$$E_{\text{coh}}^{\text{cr}} = \frac{1}{n} E_{\text{crystal}}^{\text{total}} - E_{\text{molecule}}^{\text{total}} \quad (8)$$

Table S18 Calculated Cohesive energies (kJ/mol) $E_{\text{coh}}^{\text{cr}}$, $\Delta_{\text{geom}}^{\text{cr} \rightarrow \text{g}} E$ and $\Delta_{\text{ZPE}}^{\text{cr} \rightarrow \text{g}} E$ of the DPZ, o-APN, APZ, t-PZA.

molecule	E_{coh}^{cr}	$\Delta_{geom}^{cr \rightarrow g} E$	$\Delta_{ZPE}^{cr \rightarrow g} E$	$\Delta_{sub}H$ (OK)
DPZ	-52.11	-3.22	-2.35	46.54
o-APN	-104.22	-42.07	-9.74	52.41
APZ	-39.56	17.74	-1.55	55.75
t-PZA	-65.62	26.99	-3.8	88.81

2. Quantum mechanical predictions

Politzer and coworkers have clearly established that correlations exist between the electrostatic potential of a molecule and its condensed-phase properties, including the heats of sublimation and vaporization. Functional relationships based on such correlations can be determined through the following procedure:¹¹

First, Politzer et al. recommend determining the low-energy structure of a molecule through quantum mechanical prediction, then calculating the molecular surface area (SA) for this structure. In this approach, the SA is defined to be that corresponding to the 0.001 electrons/bohr³ isosurface of the electron density.

Next, the electrostatic potential for this isosurface is used to generate two statistically based quantities, σ_{tot}^2 and v . σ_{tot}^2 is described as an indicator of the variability of the electrostatic potential on the molecular surface, and v is interpreted as showing the degree of balance between the positive and negative potentials on the molecular surface.

From these quantities, the heat of vaporization can be represented as the heat of sublimation can be represented as:

$$\Delta H(\text{Sublimation}) = a(SA)^2 + b\sqrt{\sigma_{tot}^2 v} + c \quad (9)$$

The parameters a , b , and c in the equation are determined from least-squares fitting to reliable values of the enthalpies of phase change.

Politzer et al. applied this procedure to develop a predictive tool for the heats of sublimation of 34 organic compounds. The predictions using the tool had a standard deviation of 2.5 kcal/mol from experimental values. Politzer et al. also used this tool with one developed to calculate gas-phase heats of formation to predict solid-phase heats of formation for five compounds.

Then the Betsy followed the Politzer et al. approach to develop tools to predict the heats of sublimation and vaporization of energetic materials, found that the RMS deviation of heats of sublimation from 36 experimental values is 3.6 kcal/mol¹². The sublimation enthalpies of a series of nitro-rich compounds are predicted and the deviation between the experimental and theoretical values is about ± 3.3 kcal/mol (RMS error)¹².

Table S19 The calculated SA(\AA^2), $\sigma_{tot}^2 v$ ((kcal/mol)²), $\Delta_f H_{298K}$ (kJ/mol) and $\Delta_{Sub}H$ (kJ/mol) of the pentazole, DPZ, o-APN, APZ and t-PZA.

Molecule	SA(\AA^2)	$\sigma_{tot}^2 v$ ((kcal/mol) ²)	$\Delta_{Sub}H$ (kJ/mol)
pentazole	90.47670	54.46948	66.01
DPZ	144.76037	21.31522	58.80
o-APN	122.39838	35.57314	62.76
APZ	126.16217	39.31786	67.73
t-PZA	198.60391	22.44950	92.88

4-3. The solid formation enthalpy ($\Delta_f H_{\text{solid}}$)

Table S20 The solid formation enthalpy (kJ/mol) of DPZ, o-APN, APZ and t-PZA based on DFT method

molecule	$\Delta_{\text{sub}}H$ (0K)	$\Delta_f H_{\text{gas}}$ (0K)*	$\Delta_f H_{\text{Solid}}$ (0K)
DPZ	46.54	1257.03	1210.49
o-APN	52.41	1105.84	1053.43
APZ	55.75	1040.67	984.92
t-PZA	88.81	2221.51	2132.7

* $\Delta_f H_{\text{gas}}$ (0K) is obtained based on the equation of $\Delta_f H_{\text{gas}}$ (0K) = $\Delta_f H_{\text{gas}}$ (298 K) + $\int_{298K}^{0K} C_p dT$

Table S21 The solid formation enthalpy (kJ/mol) of DPZ, o-APN, APZ and t-PZA based on Quantum mechanical predictions with PBE method

molecule	$\Delta_{\text{sub}}H$ (298K)	$\Delta_f H_{\text{gas}}$ (298K)	$\Delta_f H_{\text{Solid}}$ (298K)
DPZ	58.80	1281.21	1222.41
o-APN	62.76	1132.60	1069.84
APZ	67.73	1059.88	992.15
t-PZA	92.88	2266.00	2173.12

5. Structure-pressure relationship

5-1. Crystal elastic constants and mechanical stability

The elastic constants and Poisson ratios are calculated by using the Forcite module with the Universal forcefield to determine the mechanical flexibility and mechanical stability of the material. Choosing the task of Mechanical Properties and the quality of Ultra-fine with the method of Constant strain then the results are showed in Table S22.

The elastic constants of a material describe its response to an applied strain or, conversely, the stress required to maintain a given deformation. Both stress and strain have three tensile and three shear components. The linear elastic constants of a crystal can therefore be described using a 6×6 symmetric matrix, having 27 different components, 21 of which are independent. However, any symmetry present in the structure may reduce this number. Properties such as the bulk modulus (response to an isotropic compression), Poisson coefficient and Lamé constants can be computed from the C_{ij} matrix.

For a monoclinic crystal, the independent elastic stiffness tensor reduces to eleven components C_{11} , C_{12} , C_{13} , C_{15} , C_{22} , C_{23} , C_{25} , C_{33} , C_{35} , C_{44} , C_{46} , C_{55} and C_{66} in the Voigt notation. The well-known Born stability criteria¹³ for a monoclinic system¹⁴ are

$$C_{11} > 0, C_{22} > 0, C_{33} > 0, C_{44} > 0, C_{55} > 0, C_{66} > 0, \quad (10)$$

$$[C_{11} + C_{22} + C_{33} + 2(C_{12} + C_{13} + C_{23})] > 0 \quad (11)$$

$$(C_{35}C_{55} - C_{35}^2) > 0, (C_{44}C_{66} - C_{46}^2) > 0, (C_{22} + C_{33} - 2C_{23}) > 0, \quad (12)$$

$$[C_{22}(C_{33}C_{55} - C_{35}^2) + 2C_{23}(C_{25}C_{35} - C_{23}^2C_{55} - C_{25}^2C_{33})] > 0, \quad (13)$$

$$\{2[C_{15}C_{25}(C_{33}C_{12} - C_{13}C_{23}) + C_{15}C_{35}(C_{22}C_{13} - C_{12}C_{23}) + C_{25}C_{35}(C_{11}C_{23} - C_{12}C_{13})] - [C_{15}^2(C_{22}C_{33} - C_{23}^2) + C_{25}^2(C_{11}C_{33} - C_{13}^2) + C_{35}^2(C_{11}C_{22} - C_{12}^2) + C_{55}(C_{11}C_{22}C_{33} - C_{11}C_{23}^2 - C_{22}C_{13}^2 - C_{33}C_{12}^2 + 2C_{12}C_{13}C_{23})]\} > 0, \quad (14)$$

The computed elastic constants for DPZ ($P2_1/c$), o-APN ($C2/c$), APZ ($P2_1/c$) and t-PZA ($P2_1/c$) are shown in Table S22. There is a large degree of elastic anisotropy among the three principal directions due to $C_{11} \neq C_{22} \neq C_{33}$. All the three conditions given in eq. (12)~(14) are not simultaneously satisfied, and this clearly indicates that all these polymorphs are mechanically unstable phases. According to the phonon computation, DPZ, o-APN, APZ and t-PZA are found to be dynamically stable. However, according to the mechanical stability criteria, they are mechanically unstable. A system is mechanically unstable but dynamically stable that might be a possible indication for a metastable phase.¹⁵

Table S22 The calculated crystal elastic constants C_{ij} (in GPa), bulk modulus B (in GPa), shear modulus G (in GPa), Poisson's ratio ν , Young's modulus E (in GPa), and compressibility (TPa^{-1}) for predicted DPZ, o-APN, APZ, t-PZA. Subscript V indicates the Voigt bound, R indicates the Reuss bound and H indicates the Hill average.

Properties	DPZ ($P2_1/c$)	o-APN ($C2/c$)	APZ ($P2_1/c$)	t-PZA ($P2_1/c$)
C_{ij}	$C_{11} = 8.03$	$C_{11} = 39.22$	$C_{11} = 8.57$	$C_{11} = 7.44$
	$C_{12} = 9.33$	$C_{12} = 24.82$	$C_{12} = 5.04$	$C_{12} = 5.61$
	$C_{13} = 4.60$	$C_{13} = 17.59$	$C_{13} = 6.52$	$C_{13} = 14.77$
	$C_{15} = 2.74$	$C_{15} = -7.30$	$C_{15} = 0.48$	$C_{15} = -8.23$
	$C_{22} = 18.02$	$C_{22} = 50.95$	$C_{22} = 7.37$	$C_{22} = 7.67$
	$C_{23} = 5.26$	$C_{23} = 29.01$	$C_{23} = 3.33$	$C_{23} = 10.11$
	$C_{25} = 4.66$	$C_{25} = 4.40$	$C_{25} = 0.59$	$C_{25} = -3.73$
	$C_{33} = 6.26$	$C_{33} = 30.36$	$C_{33} = 8.96$	$C_{33} = 14.92$
	$C_{35} = -0.73$	$C_{35} = -4.13$	$C_{35} = -0.82$	$C_{35} = 3.26$
	$C_{44} = 4.10$	$C_{44} = 6.16$	$C_{44} = 1.89$	$C_{44} = 1.52$
	$C_{46} = 2.93$	$C_{46} = 1.04$	$C_{46} = 0.16$	$C_{46} = -1.79$
	$C_{55} = 4.50$	$C_{55} = 11.23$	$C_{55} = 4.29$	$C_{55} = -1.85$
	$C_{66} = 6.65$	$C_{66} = 11.15$	$C_{66} = 2.49$	$C_{66} = 5.52$
B_V	7.86	29.26	6.07	10.11

B _R	5.59	19.99	5.68	9.74
B _H	6.72	24.63	5.88	9.93
G _V	3.92	8.98	2.40	1.01
G _R	1.48	5.54	1.75	2.23
G _H	2.70	7.26	2.08	1.62
u _{xy}	0.21	0.71	0.40	1.52
u _{xz}	0.61	-0.24	0.59	-0.25
u _{yx}	0.70	0.44	0.67	0.50
u _{yz}	0.41	0.83	-0.12	0.16
u _{zx}	0.66	-0.12	0.83	-0.42
u _{zy}	0.13	0.69	-0.10	0.85
E _X	1.89	18.36	2.59	10.37
E _Y	6.21	11.46	4.34	3.44
E _Z	2.03	9.51	3.62	17.75
Compressibility	179.00	50.02	176.09	102.63

5-2. The calculated Lattice Parameters, Density, Volume, Total Energy of four crystals in the range of 0~200 Gpa

Table S23 The calculated Lattice Parameters, Density, Volume, Total Energy of the DPZ at the different pressures.

Pressure (GPa)	Parameters			Volume	Density	Total Energy(eV)	Relative Energy(eV)
	a	b	c				
0	6.11	9.27	11.17	529.49	1.76	-10808.67	0
20	5.34	8.08	9.56	342.34	2.72	-10759.54	49.13
40	5.24	7.49	9.23	298.43	3.12	-10719.85	88.82
60	5.18	7.12	9.02	272.56	3.41	-10684.33	124.34
80	5.11	6.87	8.87	254.34	3.66	-10651.50	157.17
100	5.05	6.68	8.73	240.43	3.87	-10620.66	188.01
120	4.84	6.84	8.72	227.08	4.10	-10592.91	215.76
140	4.82	6.65	8.67	217.68	4.27	-10565.17	243.50
160	4.39	7.19	7.18	202.76	4.59	-10540.59	268.08
180	5.58	5.40	8.49	192.92	4.82	-10513.43	295.24
200	5.54	5.33	8.45	188.22	4.94	-10489.64	319.03

Table S24 The calculated Lattice Parameters, Density, Volume, Total Energy of the o-APN at the different pressures.

Pressure (GPa)	Parameters			Volume	Density	Total Energy(eV)	Relative Energy(eV)
	a	b	c				
0	11.64	4.98	16.08	800.48	1.89	-17550.35	0
20	10.65	4.66	11.51	555.54	2.73	-17471.50	78.85
40	10.26	4.55	10.77	490.54	3.09	-17406.81	143.54
60	10.04	4.48	10.25	449.51	3.37	-17348.32	202.03
80	9.83	4.43	9.73	416.10	3.64	-17294.20	256.15
100	9.88	4.40	9.04	389.35	3.89	-17240.65	309.70
120	9.85	4.31	9.09	376.56	4.02	-17194.83	355.52
140	9.68	4.31	8.71	359.86	4.21	-17147.35	403.00
160	9.83	4.24	8.56	346.90	4.37	-17104.19	446.16
180	9.32	4.27	8.60	338.43	4.48	-17061.98	488.37
200	9.66	4.18	8.33	327.15	4.63	-17020.14	530.21

Table S25 The calculated Lattice Parameters, Density, Volume, Total Energy of the APZ at the different pressures.

Pressure (GPa)	Parameters			Volume	Density	Total Energy(eV)	Relative Energy(eV)
	a	b	c				
0	3.69	15.56	9.41	462.96	1.61	-8645.13	0
20	2.88	13.37	8.04	278.14	2.68	-8604.47	40.66
40	2.72	12.65	7.72	240.80	3.09	-8572.34	72.79
60	2.66	12.45	6.91	210.38	3.54	-8549.50	95.63
80	2.60	11.83	6.88	195.24	3.80	-8524.10	121.03
100	2.29	12.16	6.65	180.96	4.11	-8495.68	149.45
120	2.27	11.93	6.56	173.55	4.29	-8473.57	171.56
140	2.39	11.40	6.66	169.87	4.38	-8455.50	189.63
160	2.36	11.21	6.62	164.19	4.53	-8434.66	210.47
180	2.34	11.04	6.58	159.22	4.67	-8414.48	230.65
200	2.32	10.88	6.54	154.78	4.81	-8394.88	250.25

Table S26 The calculated Lattice Parameters, Density, Volume, Total Energy of the t-PZA at the different pressures.

Pressure (GPa)	Parameters			Volume	Density	Total Energy(eV)	Relative Energy(eV)
	a	b	c				
0	7.05	9.38	13.86	852.59	1.75	-17291.81	0
20	6.08	7.44	13.50	540.90	2.75	-17211.70	80.11
40	5.16	8.33	13.20	465.64	3.20	-17150.58	141.23
60	5.71	7.70	12.26	431.30	3.45	-17094.14	197.67
80	6.23	6.29	11.71	404.84	3.68	-17037.04	254.77
100	6.10	6.13	11.62	378.00	3.94	-16988.12	303.69
120	6.02	5.99	11.48	358.22	4.16	-16942.22	349.59
140	5.95	5.87	11.34	342.21	4.35	-16898.53	393.28
160	5.90	5.76	11.22	328.74	4.53	-16856.68	435.13
180	5.85	5.57	10.47	317.57	4.69	-16817.50	474.31
200	6.71	4.43	11.19	304.04	4.90	-16783.38	508.43

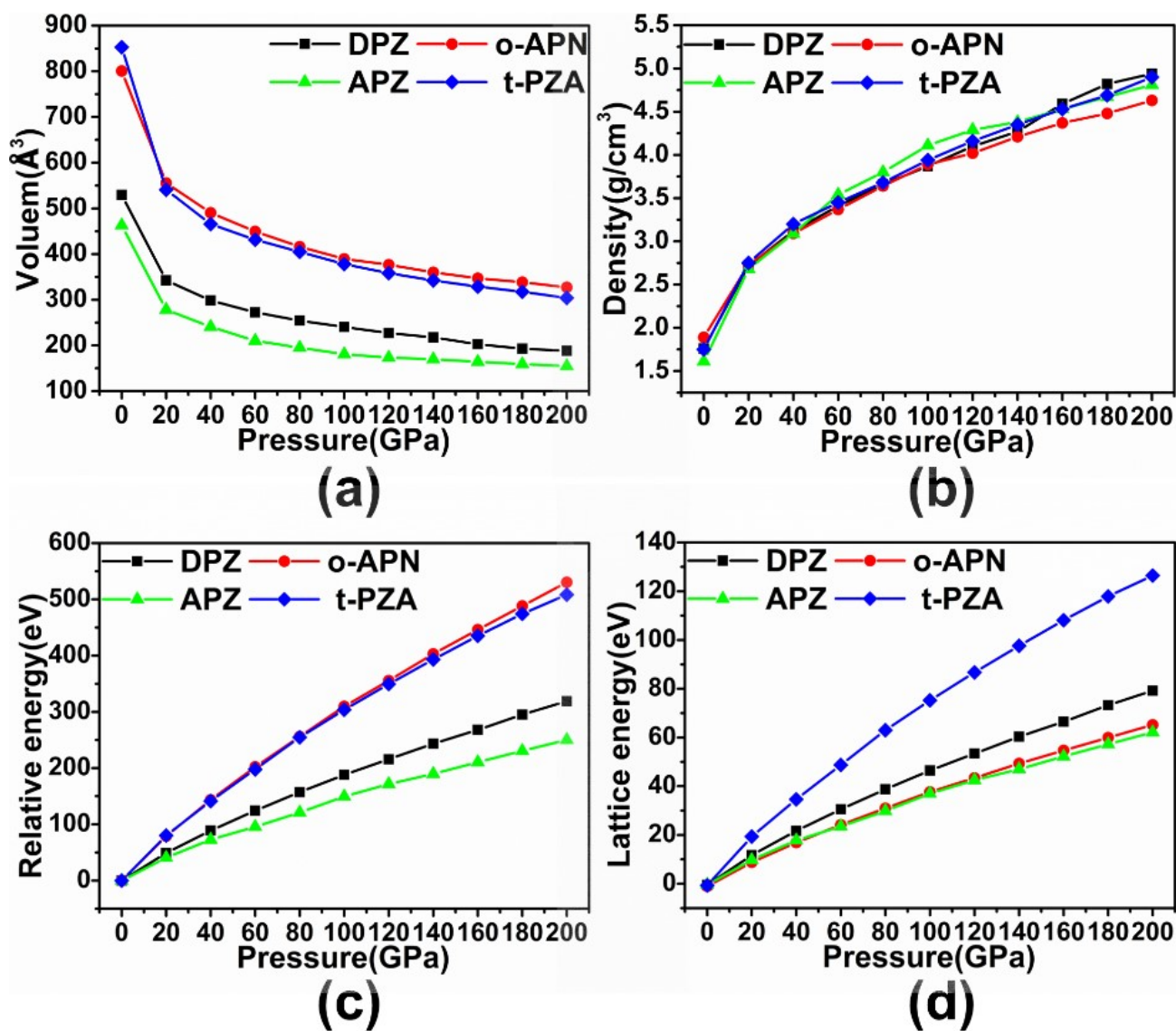


Fig S6. Calculated (a) Volume, (b) Density, (c) Relative energy, (d) Lattice energy of DPZ, o-APN, APZ and t-PZA varied with increased pressure.

5-3. Typical atom charges in four crystals under different pressures (0~200 GPa)

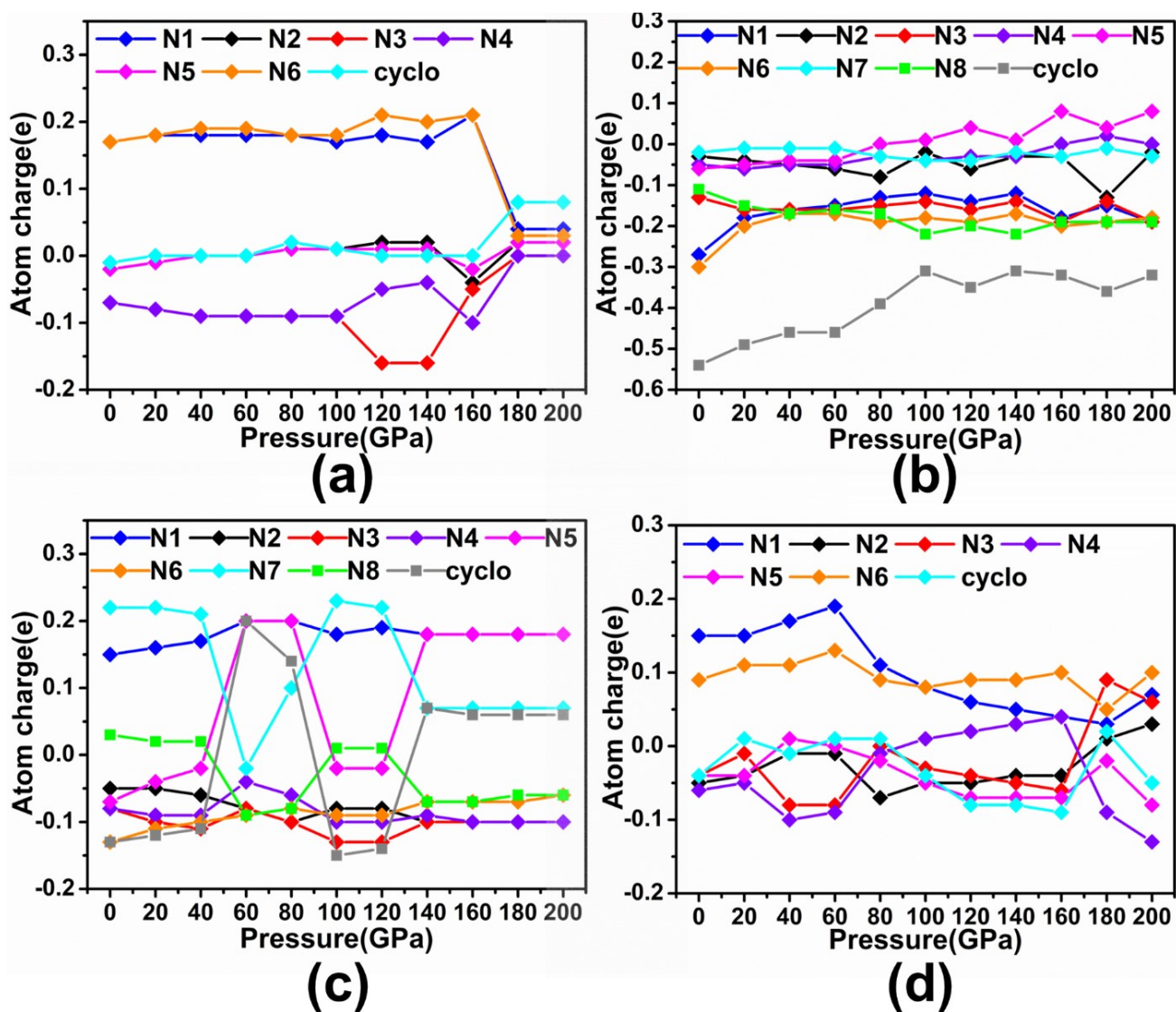


Fig S7. Calculated atom charge as a function of pressure in (a) DPZ, (b) *o*-APN, (c) APZ and (d) *t*-PZA. The cyclo represents the average charge on the ring of azole.

5-4. Band gaps of four crystals under different pressures (0~200 Gpa)

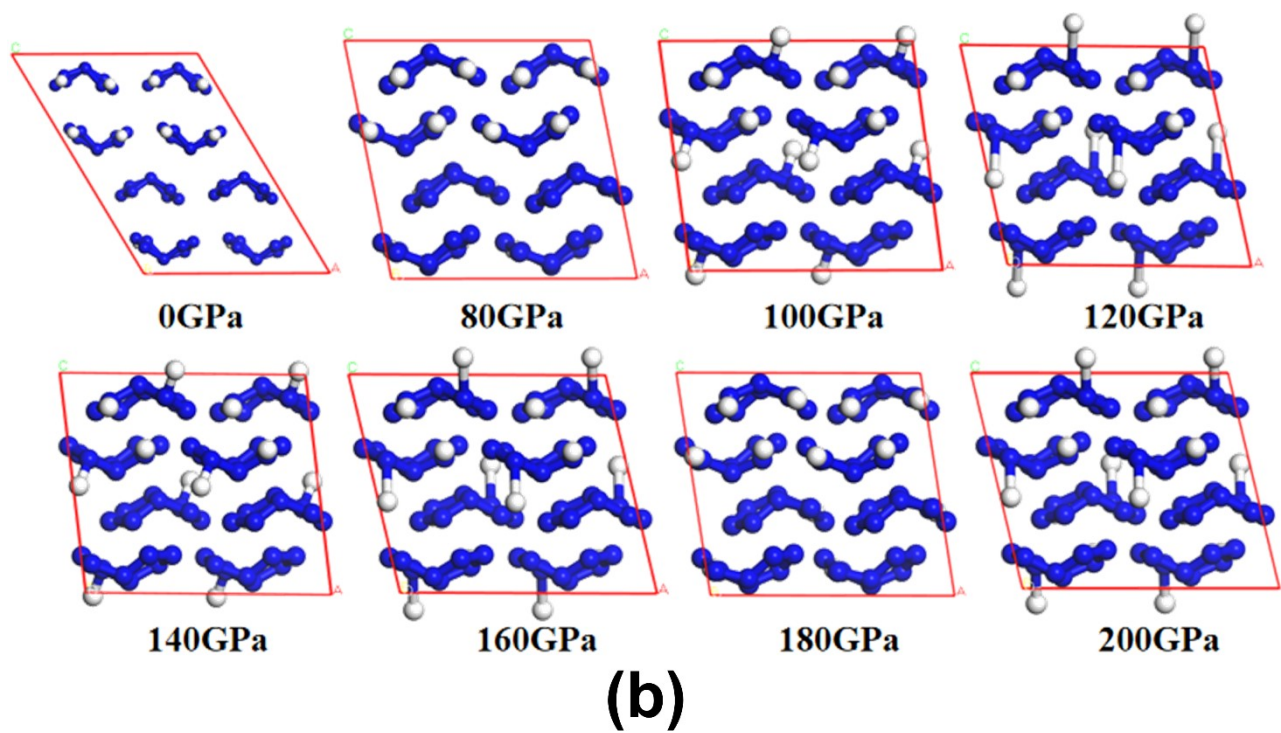
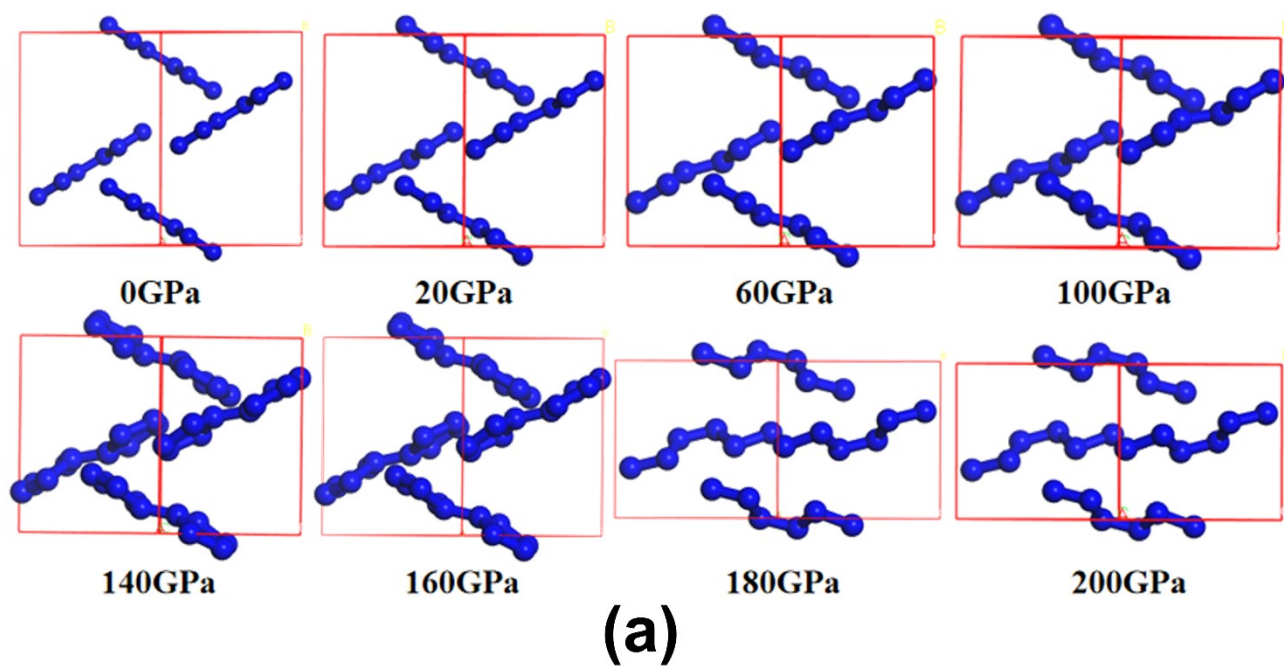
Table S27 The calculated Band gap (eV) of the DPZ, o-APN, APZ, t-PZA at the different pressures by GGA-PBE method.

Band gap (eV)	DPZ	o-APN	APZ	t-PZA
0GPa	3.653	2.189	3.250	3.839
20GPa	2.686	0.897	1.993	2.508
40GPa	2.128	0.474	1.441	2.327
60GPa	1.708	0.067	0.470	2.064
80GPa	1.374	0	0.201	1.072
100GPa	1.097	0	0	0.856
120GPa	1.003	0	0	0.503
140GPa	0.672	0	0.397	0.247
160GPa	0	0	0.358	0.024
180GPa	1.438	0	0.315	0
200GPa	1.360	0	0.295	0

Table S28 The calculated Band gap (eV) of the DPZ, o-APN, APZ, t-PZA at the different pressures by HSE06 method.

Band gap (eV)	DPZ	o-APN	APZ	t-PZA
0GPa	5.304	3.662	4.448	5.511
20GPa	4.322	1.976	2.932	3.966
40GPa	3.59	1.422	2.369	3.741
60GPa	3.081	0.867	1.776	3.355
80GPa	2.657	0	0.21	2.229
100GPa	2.324	0	0	2.039
120GPa	1.761	0	0	1.225
140GPa	1.341	0	0.462	1.264
160GPa	0.037	0	0.351	0.579
180GPa	3.421	0	0.133	0.215
200GPa	3.352	0	0	0

5-5. Structure change of four crystals under different pressures (0~200 Gpa)



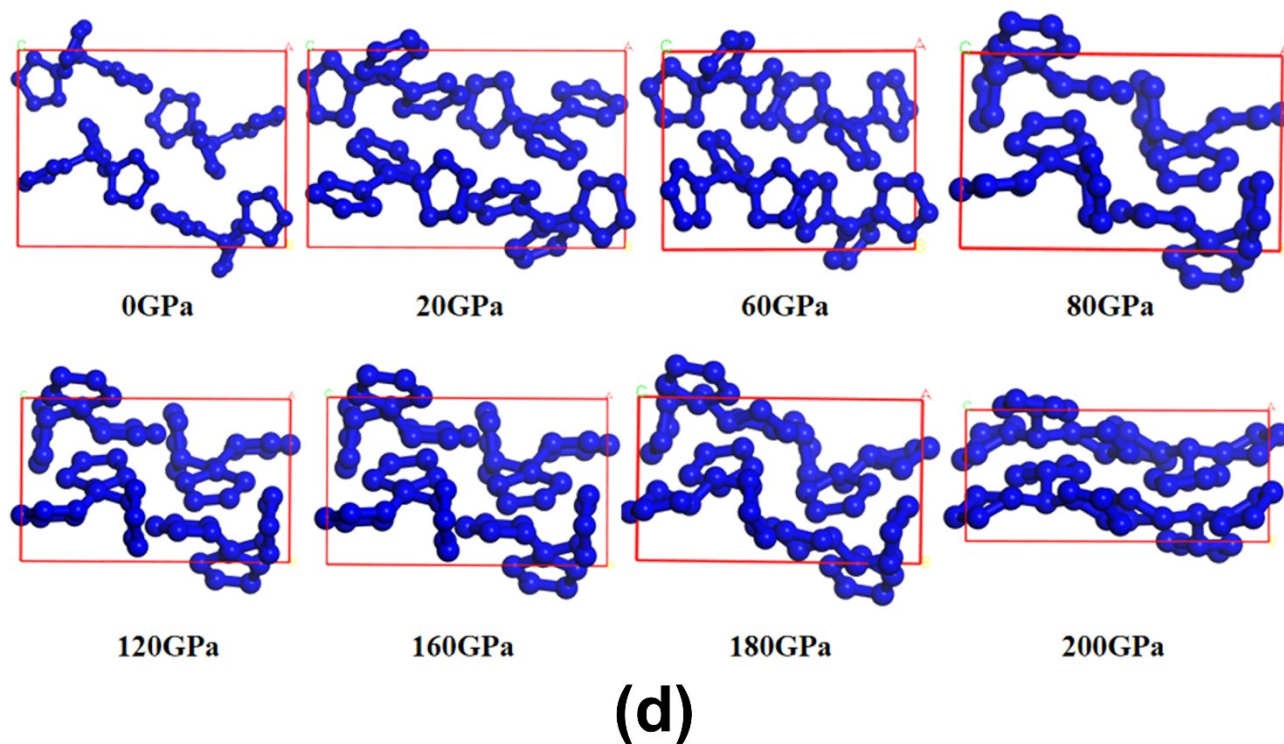
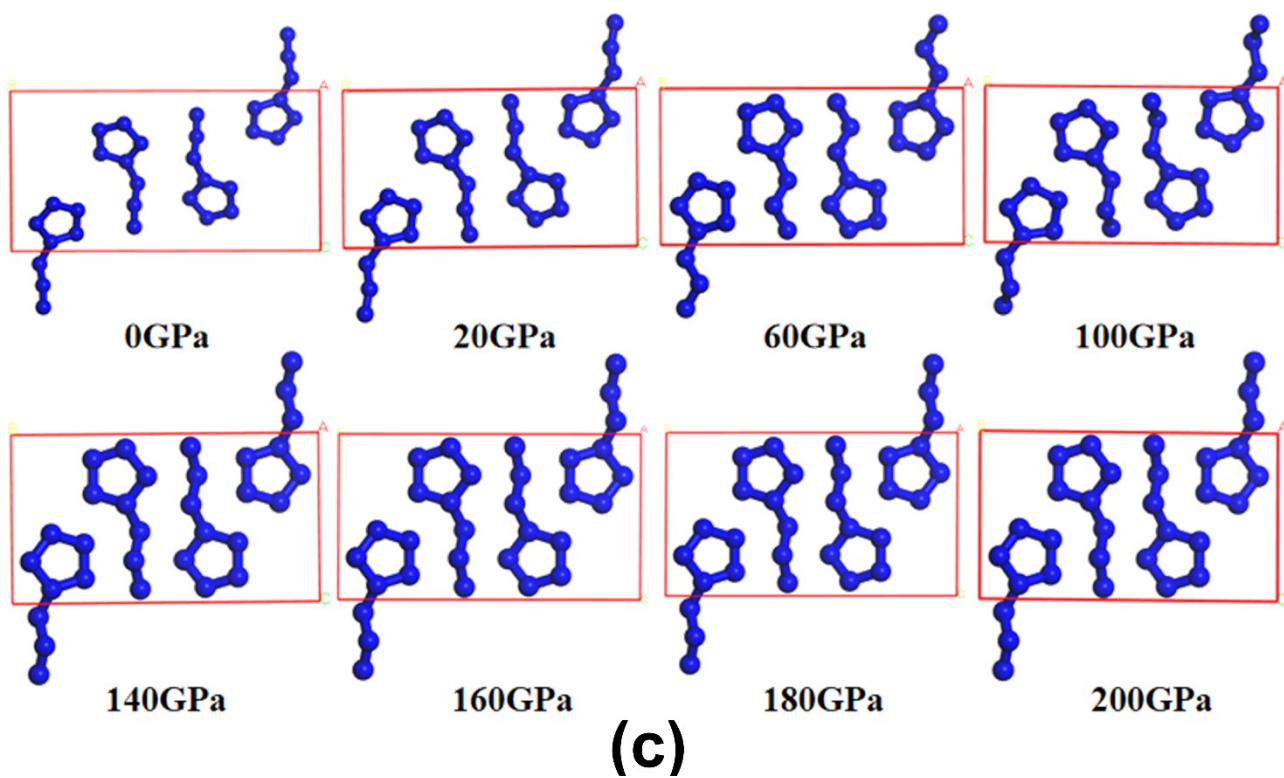


Fig S8. Calculated changes of crystal structures as a function of pressure in (a) DPZ, (b) *o*-APN, (c) APZ and (d) *t*-PZA.

5-6 Formation Gibbs free energy (defined) at ambient and high pressure.

The Gibbs free energy based on the definition of $\Delta_r G_m = G(\text{crystal}) - n G(\text{molecule})$ at the pressures of metallization and phase transition, where n is the number of the molecules. We have built $30 \times 30 \times 30 \text{ \AA}$ box for calculating the energy of molecules. As comparison, the defined $\Delta_r G_m$ (kcal/mol) at ambient pressure are also calculated.

Table S29 The calculated Gibbs free energy of crystal and molecule at different pressure

Structure	G (crystal)/eV	G(molecule)/eV	$\Delta_r G_m$ (eV)	$\Delta_r G_m$ (kcal/mol)
DPZ-0 Gpa	-10808.67	-2701.62	-2.17	-51.99
DPZ-160 GPa	-10806.30	-2701.57	-0.03	-0.72
DPZ-180 GPa	-10773.80	-2692.02	-5.72	-137.05
o-APN-0 GPa	-17550.35	-2192.71	-8.67	-207.73
o-APN-80 GPa	-17545.55	-2193.24	0.36	8.63
o-APN-100 GPa	-17544.53	-2193.32	2.09	50.08
APZ-0 GPa	-8645.13	-2160.87	-1.65	-39.53
APZ-120 GPa	-8642.58	-2160.61	-0.14	-3.35
APZ-140 GPa	-8641.01	-2160.16	-0.36	-8.63
t-PZA-0 GPa	-17291.81	-4322.27	-2.73	-65.41
t-PZA-80 GPa	-17287.58	-4321.91	0.04	0.96
t-PZA-180 GPa	-17285.22	-4318.87	-9.74	-233.37

6. Molecular dynamics simulations with NPT ensemble

6-1. Atomic charges of the four structures preparing for MD simulation at ambient pressure

Table S30 The Mulliken atomic charges of the four structures preparing for MD simulation at ambient pressure.

Atomic charge	N1	N2	N3	N4	N5	N6	N7	N8
DPZ	0.60	-0.27	-0.029	-0.028	-0.27	0.60	--	--
o-APN	-0.25	+0.045	-0.053	0.053	-0.040	-0.078	-0.045	-0.12
APZ	1.02	-0.29	-0.10	-0.047	-0.40	-0.65	0.70	-0.23
t-PZA	0.56	-0.18	-0.066	-0.067	-0.18	0.55	--	--

Table S31 The CHELPG atomic charges of the four structures at ambient pressure

Atomic charge	N1	N2	N3	N4	N5	N6	N7	N8
DPZ	0.60	-0.27	-0.029	-0.028	-0.27	0.60	--	--
o-APN	-0.25	+0.045	-0.053	0.053	-0.040	-0.078	-0.045	-0.12
APZ	1.02	-0.29	-0.10	-0.047	-0.40	-0.65	0.70	-0.23
t-PZA	0.56	-0.18	-0.066	-0.067	-0.18	0.55	--	--

6-2. Energy-time curves of the four predicted crystals at ambient pressure (300 K and 500 K).

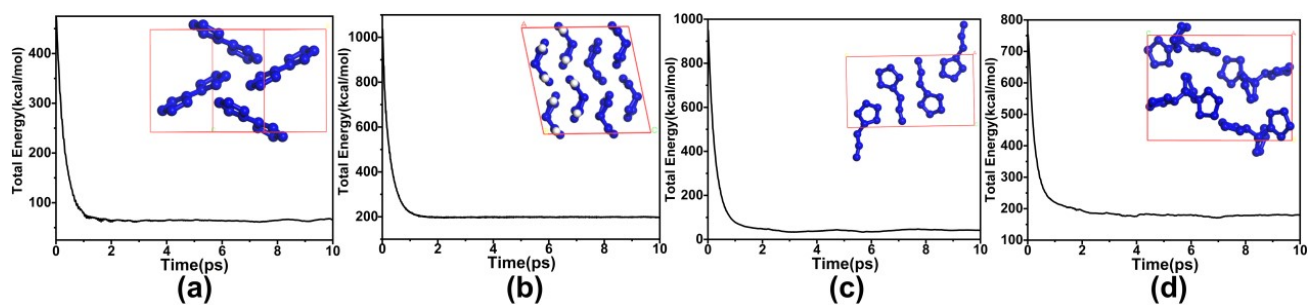


Fig. S9 NPT molecular dynamic studies for the four crystals under the ambient pressure at 300 K. (a) DPZ, (b) o-APN, (c) APZ and (d) t-PZA, with the final crystal structures at equilibrium states.

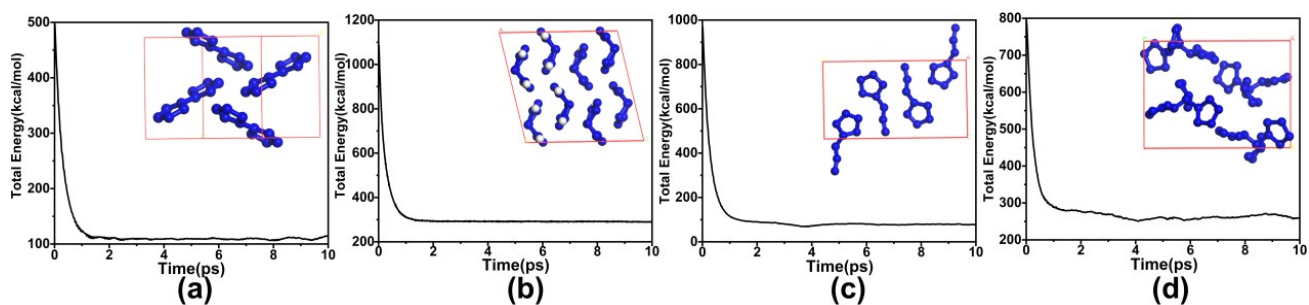


Fig. S10 NPT molecular dynamic studies for the four crystals under the ambient pressure at 500 K. (a) DPZ, (b) o-APN, (c) APZ and (d) t-PZA, with the final crystal structures at equilibrium states.

6-3. The converged dynamic temperature of the four crystals at the pressure of phase transition.

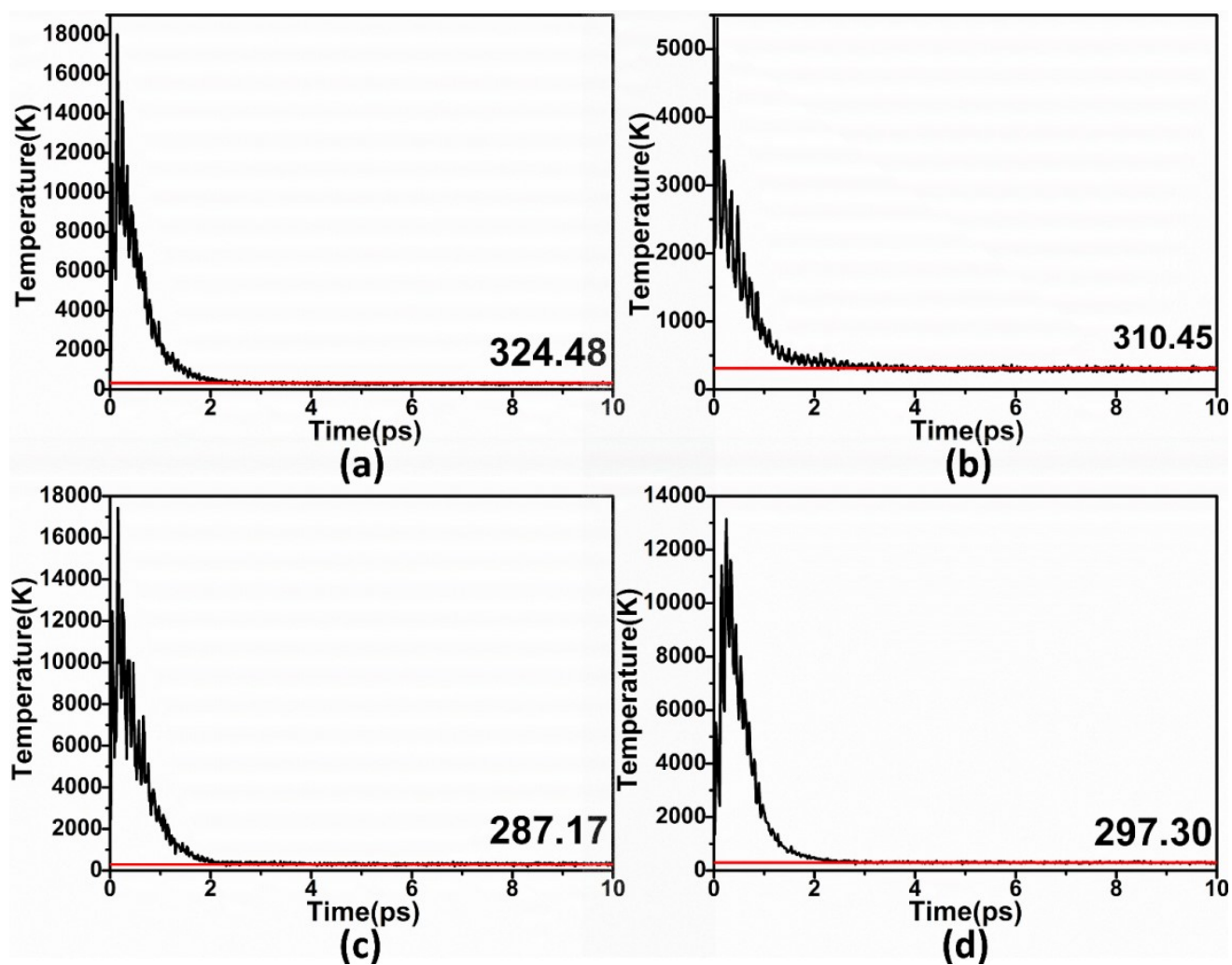


Fig S11. NPT molecular dynamic studies for the four crystals at the pressure of phase transition. (a) DPZ (180 Gpa), (b) o-APN (80 Gpa), (c) APZ (140 Gpa), (d) t-PZA (180 Gpa), with the converged dynamic temperature (red line).

6-4. Converged potential energy, kinetic energy, non-bond energy and total energy.

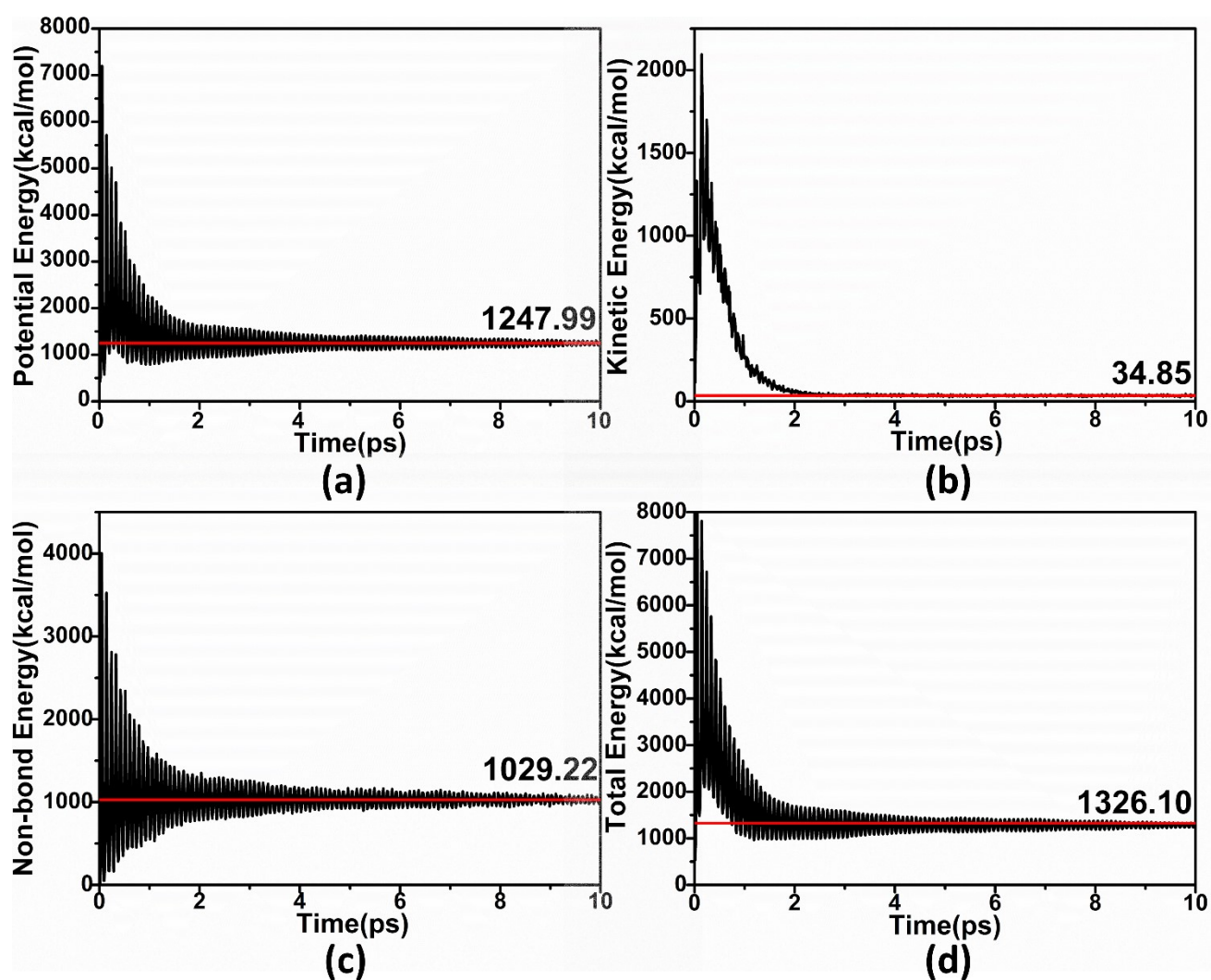


Fig S12. NPT molecular dynamic studies for the DPZ (180 Gpa) at the pressure of phase transition. (a) Potential energy, (b) Kinetic energy, (c) Non-bond energy, (d) Total energy, with the converged dynamic energy (red line).

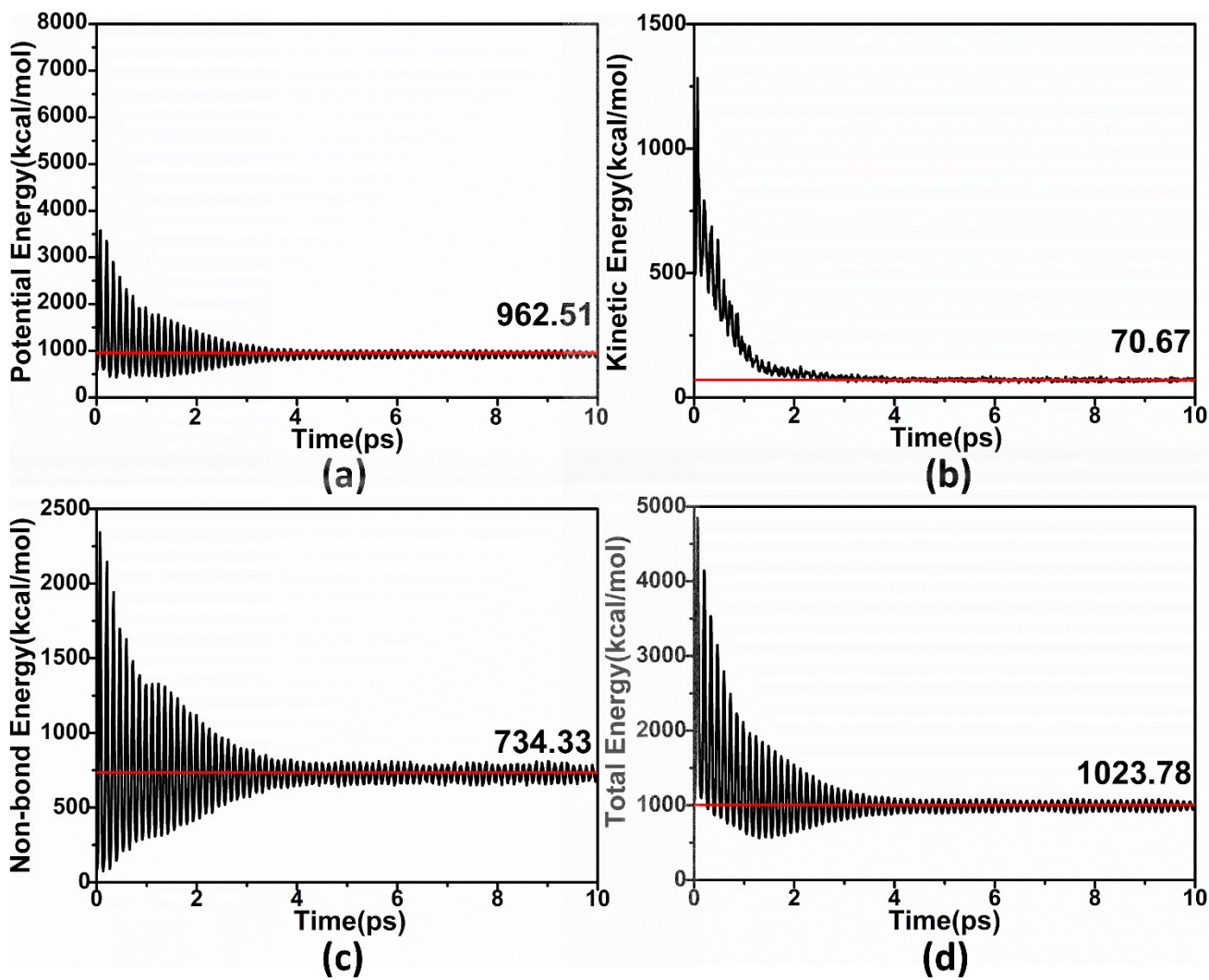


Fig S13. NPT molecular dynamic studies for the o-APN (80 Gpa) at the pressure of phase transition. (a) Potential energy, (b) Kinetic energy, (c) Non-bond energy, (d) Total energy, with the converged dynamic energy (red line).

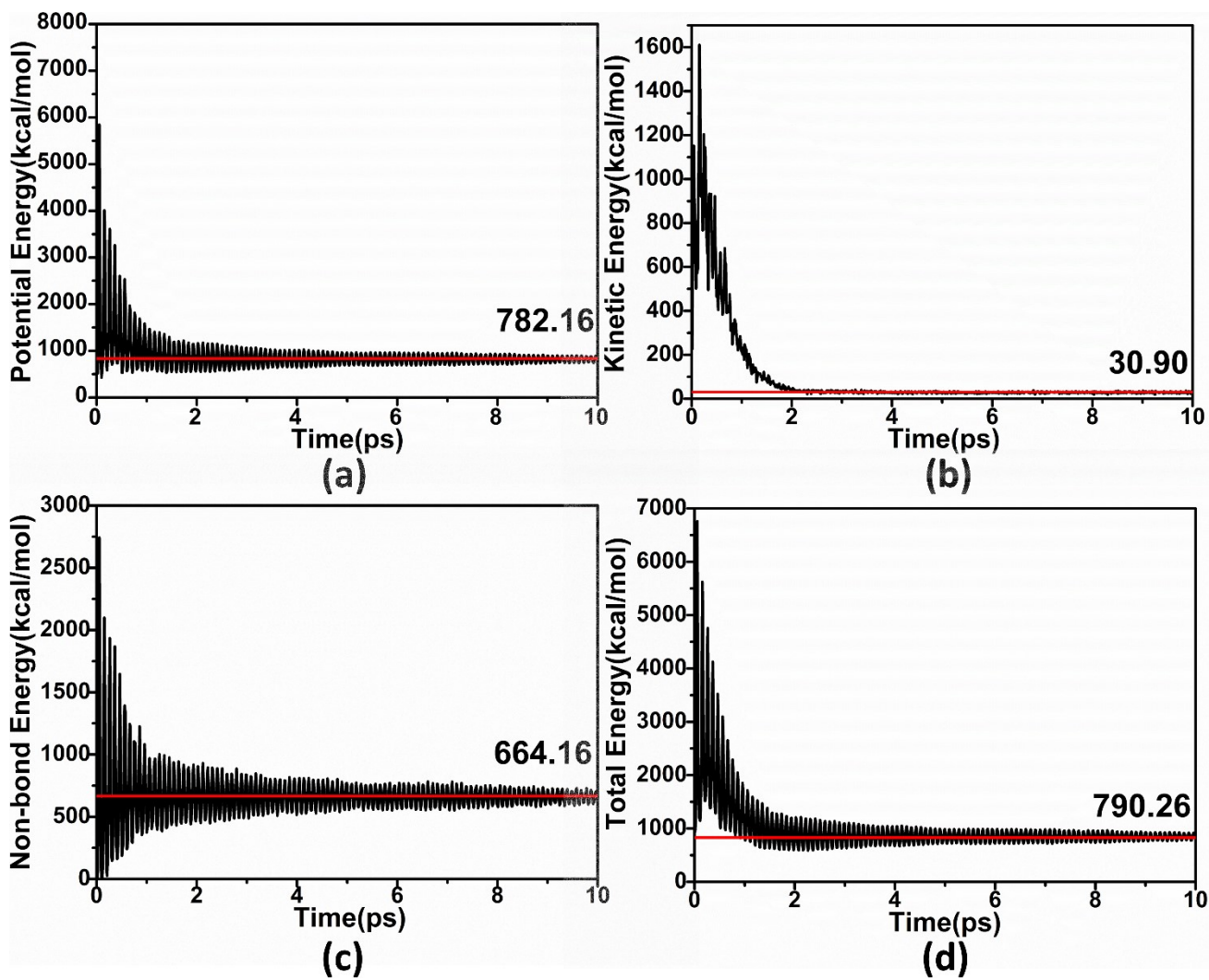


Fig S14. NPT molecular dynamic studies for the APZ (140 GPa) at the pressure of phase transition. (a) Potential energy, (b) Kinetic energy, (c) Non-bond energy, (d) Total energy, with the converged dynamic energy (red line).

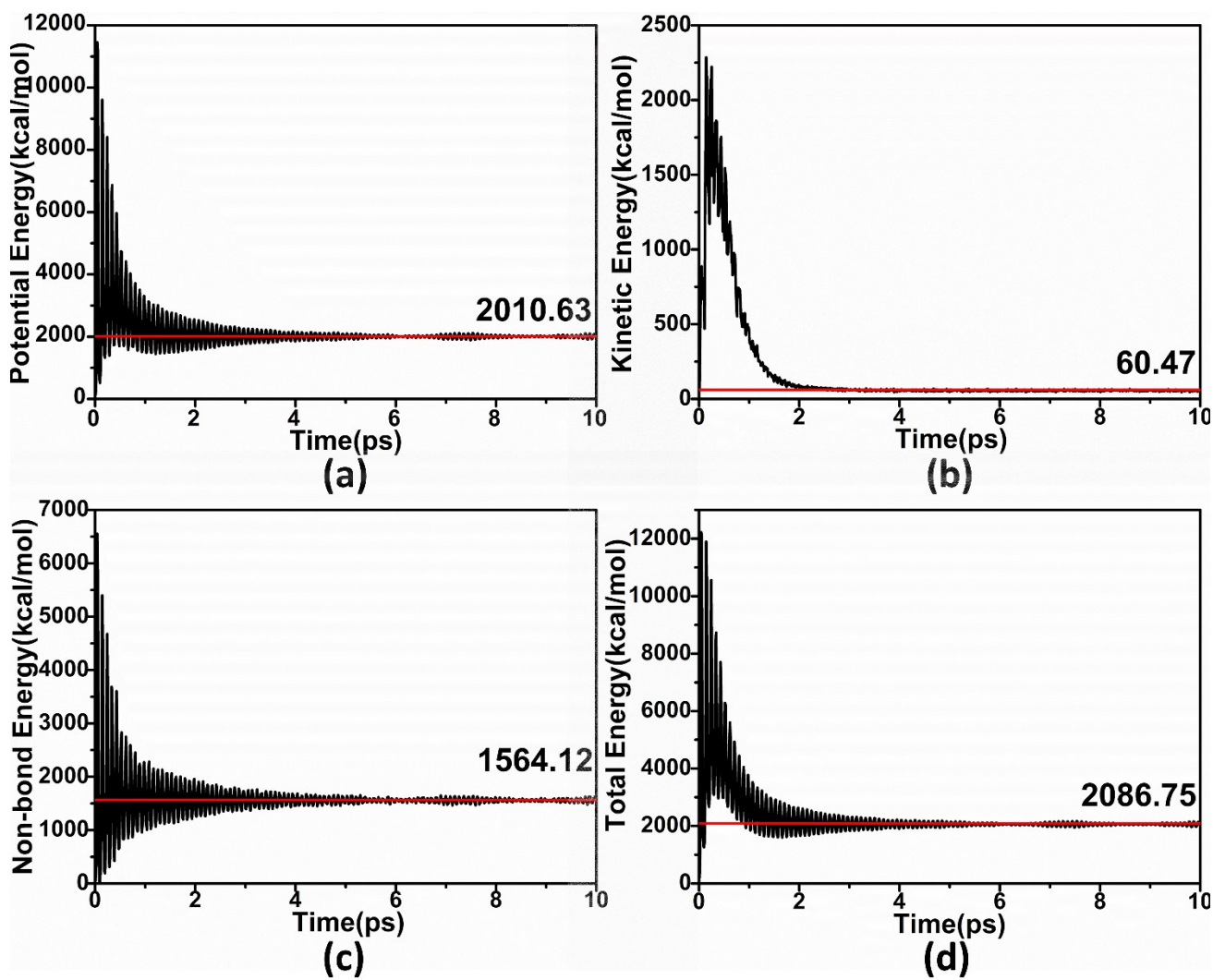


Fig S15. NPT molecular dynamic studies for the t-PZA (180 Gpa) at the pressure of phase transition. (a) Potential energy, (b) Kinetic energy, (c) Non-bond energy, (d) Total energy, with the converged dynamic energy (red line).

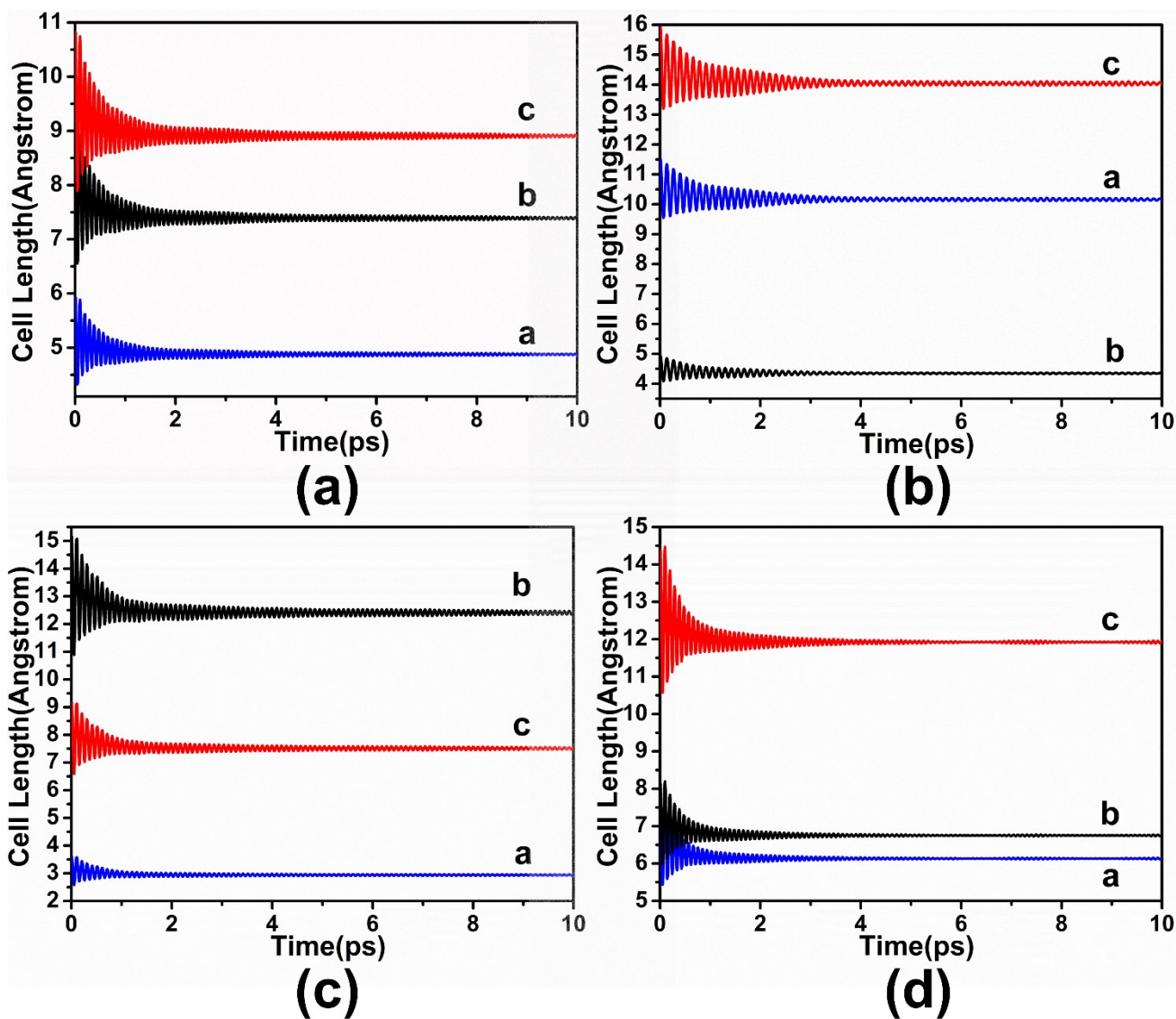


Fig S16. NPT molecular dynamic studies for the four crystals at the pressure of phase transition. (a) DPZ (180 Gpa), (b) o-APN (80 Gpa), (c) APZ (140 Gpa), (d) t-PZA (180 Gpa), with the converged cell length (Å).

References

1. W. Yang and R. G. Parr, *PNAS*, 1985, **82**, 6723-6726.
2. N. Blagden and R. J. Davey, *Cryst. Growth. Des.*, 2003, **3**, 873-885.
3. V. Belsky and P. Zorkii, *Acta Crystallogr. Sect. A: Found. Crystallogr.*, 1977, **33**, 1004-1006.
4. A. K. Rappé, C. J. Casewit, K. Colwell, W. A. Goddard III and W. M. Skiff, *J. Am. Chem. Soc.*, 1992, **114**, 10024-10035.
5. Y. Liu, H. Du, L. Fang, F. Sun, H. Su, Z. Ge, W. Guo and J. Zhu, *RSC adv.*, 2021, **11**, 21507-21513.
6. H. Fujihisa, K. Honda, S. Obata, H. Yamawaki, S. Takeya, Y. Gotoh and T. Matsunaga, *CrystEngComm*, 2011, **13**, 99-102.
7. H. Sun, *J. Phys. Chem. B*, 1998, **102**, 7338-7364.
8. S. L. Mayo, B. D. Olafson and W. A. Goddard, *J. Phys. Chem.*, 1990, **94**, 8897-8909.
9. J. W. Ochterski, *Gaussian Inc*, 2000, **1**, 1-19.
10. C. Červinka and M. Fulem, *J. Chem. Theory Comput.*, 2017, **13**, 2840-2850..
11. P. Politzer, J. S. Murray, M. Edward Grice, M. Desalvo and E. Miller, *Mol. Phys.*, 1997, **91**, 923-928.
12. B. M. Rice, S. V. Pai and J. Hare, *Combust. Flame*, 1999, **118**, 445-458.
13. F. I. Fedorov, *Theory of Elastic Waves in Crystals*, Plenum, New York, 1968, p. 33
14. J. F. Nye, *Physical Properties of Crystals*, Oxford University Press, Oxford, 1985
15. P. Vajeeston and H. Fjellvåg, *RSC advances*, 2017, **7**, 16843-16853.